Pontifícia Universidade Católica
do Rio de Janeiro

Pedro Henrique de Lima Ripper Moreira

Thermodynamic model for VLE water - MDEA system: Peng-Robinson and Uniquac models.

Dissertação de Mestrado

Dissertation presented to the Programa de Pós-graduação em Engenharia Química, de Materiais e Processos Ambientais of PUC-Rio in partial fulfillment of the requirements for the degree of Mestre em Engenharia Química, de Materiais e Processos Ambientais.

Advisor: Prof. Rogério Navarro Correia de Siqueira

Rio de Janeiro

March 2023

Pontifícia Universidade Católica do Rio de Janeiro

Pedro Henrique de Lima Ripper Moreira

Thermodynamic model for VLE water - MDEA system: Peng-Robinson and Uniquac models.

Dissertation presented to the Programa de Pós–graduação em Engenharia Química, de Materiais e Processos Ambientais of PUC-Rio in partial fulfillment of the requirements for the degree of Mestre em Engenharia Química, de Materiais e Processos Ambientais. Approved by the Examination Committee.

Prof. Rogério Navarro Correia de Siqueira

Advisor

Departamento de Engenharia Química e de Materiais – PUC-Rio

Prof. Roberto Ribeiro de Avillez

Departamento de Engenharia Química e de Materiais – PUC-Rio

Prof. Fernando Luiz Pellegrini Pessoa

Centro de Competências em Intensificação de Processos – SENAI-CIMATEC

Rio de Janeiro, March 24th, 2023

Pedro Henrique de Lima Ripper Moreira

Graduated in Chemistry and Chemical Engineering at PUC-Rio (Pontifical Catholic University of Rio de Janeiro) in 2018.

Bibliography Data

Moreira, Pedro Henrique de Lima Ripper

Thermodynamic model for VLE water - MDEA system: Peng-Robinson and Uniquac models / Pedro Henrique de Lima Ripper Moreira ; advisor: Rogério Navarro Correia de Siqueira. – 2023.

66 f. ; 30 cm

Dissertação (mestrado)–Pontifícia Universidade Católica do Rio de Janeiro, Departamento de Engenharia Química e de Materiais, 2023.

Inclui bibliografia

1. Engenharia Química e de Materiais – Teses. 2. Termodinâmica. 3. Equilíbrio líquido vapor. 4. Pressão de bolha. 5. Peng – Robinson. 6. UNIQUAC. I. Siqueira, Rogério Navarro Correia de. II. Pontifícia Universidade Católica do Rio de Janeiro. Departamento de Engenharia Química e de Materiais. III. Título.

CDD: 620.11

Acknowledgments

To my parents, Denise and Pedro Paulo, for their support and trust, which greatly contributed to the completion of this work.

To my advisor Rogério Navarro, for his willingness and patience during these difficult months resulting from the COVID-19 pandemic.

To my friends, who encouraged me in difficult times and understood my absence while I was dedicated to carrying out this work.

To the Human Resources Program of the National Petroleum Agency, PRH-ANP, for granting me a scholarship to carry out my research.

To the professors who participated in the examining committee.

To everyone who participated, directly or indirectly, in the development of this research work, enriching my learning process.

To PUC-Rio, essential in my professional training process, for their dedication and for everything I learned over the years of the course.

This study was financed in part by the Coordenação de Aperfeiçoamento de Pessoal de Nível Superior - Brasil (CAPES) - Finance Code 001.

Abstract

Moreira, Pedro Henrique de Lima Ripper; Siqueira, Rogério Navarro Correia (Advisor). **Thermodynamic model for VLE water - MDEA system: Peng-Robinson and Uniquac models.** Rio de Janeiro, 2023. 66p (paginas). Dissertação de Mestrado – Departamento de Engenharia Química e de Materiais, Pontifícia Universidade Católica do Rio de Janeiro.

Determining interaction parameter for equations of state (EOS) of water – amines systems are crucial to develop accurate models in chemical engineering processes. The binary system of N-methyldiethanolamine (MDEA) and water in biogas purification was evaluated using both φ – φ and γ – φ approaches, classic Peng–Robinson with the empirical "non-random" mixing rule and Peng–Robinson with the Wong-Sandler mixing rule EOS to optimize pure components acentric factor, ω, and binary interaction parameters, k_{ij}. The interaction parameters u_{ij} from EOS that incorporate UNIQUAC model, such as γ – φ approach and Wong-Sandler mixing rule were optimized as well. These parameters were evaluated using a bubble pressure algorithm, MATLAB coding and minimization of objective functions related to absolute average deviation, AAD, between experimental and calculated data at different temperatures. The calculated ω of water, CO_2 and MDEA were 0.3275, 0.2039 and 1.0133 respectively with lower AAD than literature values. The $\varphi - \varphi$ approach classic Peng–Robinson with Wong – Sandler mixing rule EOS was better suited for the MDEA – H_2O binary, resulting in as $u_{12}^0 = -234.2841$, $u_{12}^T = 1.0499$, $u_{21}^0 = 266.4326$, $u_{21}^T = 0.1966$, $k_{ij} = -0.0715$, with vapor pressure AAD% = 6.57% and composition AAD% = 17.51%. Due to the highly non-ideal nature of the CO_2 – H_2O binary system, neither φ – φ or γ – φ approaches using the selected EOS resulted in accurate vapor – liquid equilibrium (VLE) bubble point pressure diagrams.

Keywords

Bubble pressure; Amine; Thermodynamic modelling; Equilibrium; Peng-Robinson; UNIQUAC; Wong – Sandler

Resumo

Moreira, Pedro Henrique de Lima Ripper; Siqueira, Rogério Navarro Correia. **Modelo termodinâmico para ELV do sistema água - MDEA: modelos de Peng-Robinson e Uniquac.** Rio de Janeiro, 2023. 66p (paginas). Dissertação de Mestrado – Departamento de Engenharia Química e de Materiais, Pontifícia Universidade Católica do Rio de Janeiro.

A determinação de parâmetros de interação precisos para equações de estado (EdE) em sistemas aquosos de aminas são cruciais para desenvolver modelos termodinâmicos em processos da engenharia química. O sistema binário de N-metildietanolamina (MDEA) e água na purificação do biogás foi avaliado usando as abordagens $\varphi - \varphi$ e $\gamma - \varphi$, EdE de Peng–Robinson clássico com a regra de mistura não aleatória e EdE Peng–Robinson com a regra de mistura Wong-Sandler, para otimizar o fator acêntrico, ω, de componentes puros, e os parâmetros de interação binária, k_{ij}. Os parâmetros de interação u_{ij} das EdE que incorporam o modelo UNIQUAC, como a abordagem γ – φ e a regra de mistura de Wong-Sandler também foram otimizados. Esses parâmetros foram avaliados usando um algoritmo de pressão de bolha reativa, codificação MATLAB e minimização de funções objetivas relacionadas ao desvio médio absoluto, AAD, entre dados experimentais e calculados em diferentes temperaturas. Os ω calculados de água, CO2 e MDEA foram 0,3275, 0,2039 e 1,0133, respectivamente, com AAD inferior aos valores da literatura. A abordagem $\varphi - \varphi$ com EdE clássica de Peng–Robinson com regra de mistura Wong–Sandler foi mais adequada para o binário MDEA – H2O, resultando em $u_{12}^{0} = -234.2841$, $u_{12}^{T} = 1.0499$, $u_{21}^{0} = 266.4326$, $u_{21}^{T} = 0.1966$, $k_{ij} = -0.0715$, com pressão de vapor AAD% = 6,57% e composição AAD% = 17,51%. Devido à natureza altamente não ideal do sistema binário CO2 – H2O, nem as abordagens φ – φ ou γ – φ usando as EdE selecionadas resultaram em diagramas precisos de pressão de ponto de bolha para o equilíbrio vapor – líquido (VLE).

Palavras-chave

Termodinâmica; equilíbrio líquido vapor; pressão de bolha; Peng – Robinson; UNIQUAC; Wong – Sandler

Summary

List of Figures

List of Tables

List of Abbreviations

Abbreviation	Definition
AAD	Absolute average deviation
ARD	Absolute relative deviation
EOS	Equation of State
MDEA	N-methyldiethanolamine
NRTL	Non-random two liquid model
PR	Peng - Robinson
PR-EOS	Peng - Robinson equation of state
PRNR-EOS	Peng - Robinson with "non-random" mixing rule equation of state
PRWS-EOS	Peng - Robinson with Wong - Sandler's mixing rule equation of state
SRK	Soave - Redlich - Kwong
UNIQUAC	Universal Quasi - Chemical model
VLE	Vapor - liquid equilibrium
WS	Wong - Sandler

1. Introduction

Biogas is a renewable energy source that comes from the breakdown, by anaerobic digestion, of organic waste materials such as food scraps, animal manure, and sewage sludge. Its production systems help to reduce the amount of waste going to landfills and can reduce odors and other environmental impacts associated with waste handling. Unlike fossil fuels, which are finite resources, biogas can be continuously produced as long as there are organic materials to feed into the system, granting it the characteristic of being a renewable energy source (Parsaee, 2019). Since its production captures methane gas that would otherwise be released into the atmosphere, it is an important asset for the reduction of a significant portion of greenhouse gas emissions. It plays a fundamental role in Brazilian agrobusiness, providing a source of renewable energy and animal waste management. This can reduce reliance on fossil fuels and chemical fertilizers, supporting more sustainable agricultural practices (Junior, 2022). Overall, biogas production offers a number of benefits, including renewable energy, reduced greenhouse gases, waste management, and support for sustainable agriculture.

Biogas purification leads to the production of biomethane, a refined gas with high methane, CH_4, which has characteristics that make it interchangeable with natural gas in all its applications (ANP, 2017). However, the composition of biogas can vary depending on the feedstock used, temperature, pH, and other factors, making it difficult to design a purification system that works consistently. It also contains impurities such as carbon dioxide, CO_2, hydrogen sulfide, H_2S, water vapor, and trace amounts of other gases, some of which, like hydrogen sulfide, can be corrosive and damage the pipeline and equipment used to transport and process the gas (Okamura, 2018). The combustion of H_2S results in the production of SO_2 and SO_3, both highly toxic gases that endanger the life of the processing plant operator. Among the pollutants, CO_2 is the one with the highest composition, but due to its inert quality in combustion, it reduces the amount of heat generated from biogas.

The most widely used H_2S and CO_2 removal process is the water scrubbing process, in which, countercurrent water comes into contact with brute biogas in an absorption column, where the components of the gas phase can either react (chemical

absorption) or dissolve (physical absorption) with the solvent. Even though water has shown effectiveness regarding their removal, its reaction with H_2S generates sulfuric acid, which requires further treatment to be safely removed (Oliveira, 2022). An alternative method to solve this problem is the amine scrubbing process, where CO_2 is absorbed both physically and chemically by an amine-based solution, which depending on the selected amine, could display capability of simultaneous H_2S removal (Abdeen, 2016). Therefore, biogas purification is a complex and challenging process that requires careful consideration of the composition of the gas and the environmental impacts of the purification process.

Developing an understanding of transfer phenomena and accurate thermodynamic models is crucial for properly simulating absorption/stripping processes involving amine aqueous solvents. This is because successful simulation, design, and optimization of CO_2 and H_2S capture hinges on the modeling of thermodynamic properties like vapor-liquid equilibrium (VLE) and chemical reaction equilibrium. These require the appropriate selection and understanding of equations of state, capable of predicting accurate and non-ideal system properties, and equilibrium approach, relying only on concepts of fugacity coefficient to model system phases ($\varphi - \varphi$ approach) or modelling the liquid phase using activity coefficient models ($\gamma - \varphi$ approach). Similarly, the availability of reliable experimental data is critical for precise thermodynamic modeling and interaction parameter optimization. While there is an abundance of experimental data on water – amine systems, recent literature reviews have identified some questionable published CO_2 solubility data for aqueous amine systems. This results in great inaccuracies regarding the predicted and experimental data, which can be aggravated by the fact that, in general, authors apply their thermodynamic models directly to a complex system, without first applying their model to its simpler counterparts.

2. Main Objectives

The purpose of this work is to create a scalable thermodynamic model using MATLAB coding, capable of accurately predicting the vapor – liquid equilibrium, at different pressure and temperature conditions, for biogas purification systems. The selected amine solvent was N-methyldiethanolamine, also known as MDEA, for its ternary amine capacity to simultaneously remove CO_2 and H_2S from the gas phase (Moreira, 2022).

The classic Peng – Robinson equation of state, PR-EOS with two different interaction mixture rules, the empirical "non-random", PRNR-EOS, and Wong – Sandler's mixing rules, PRWS-EOS, were modelled using both $\varphi - \varphi$ and $\gamma - \varphi$ approaches, as to determine parameter values for more accurate models. The excess Gibbs energy model used for the Wong Sandler mixing rule and activity coefficient calculations was the UNIQUAC model. The UNIQUAC size parameters, r_i and q_i will be obtained by following the group contribution method as described by Sandler, 2017.

This model will start from the simpler pure component systems of water, CO_2 and MDEA to optimize acentric factor parameters for binary systems. The binary system MDEA-water was modeled and all parameters were optimized following a predictive bubble pressure algorithm for their corresponding selected equation of state, EOS, and approaches.

The strategy for parameter optimization is detailed on further sections. All predicted data was compared to experimental data using absolute average deviation, AAD and absolute relative deviation, ARD, as a metric of accuracy.

3. Literature Review

The selection of an appropriate economically viable purification technique for the simultaneous removal of CO_2 and H_2S is vital to encourage development of biogas production technologies. Since water scrubbing applied to biogas results in the production of sulfuric acid byproducts, the amine scrubbing has been looked upon as an alternative to solve this issue. Gamba et al., 2014, used a mixture of 15% MEA and 50% MDEA in a pall rings packed column reactor to purify a feed biogas of composition 58% CH_4 and 36.6% CO_2, reporting a biomethane composition of 98% CH_4 and <2% CO_2, with lower power consumption caused by using MDEA. Peralta, 2013, used 10% MEA in polyethylene jacks packed column reactor to obtain biomethane purity of 90% CH_4, <10% CO_2 and <100 ppm H_2S concentrations, which shows that more sterically hindered amines are potentially better for CO_2 removal from the gas mixtures. To corroborate that, Günther, 2012, used 20% DEA solvent on a plastic polypropylene packed column reactor to purify a feed biogas of 51.1% CH_4, 46% CO_2 and 80 ppm H_2S into a product of purity 98.4% CH_4, 0.1% CO_2 and 0.1 ppm H_2S. Also, Gaur et al., 2010, used a blend of 30% MEA and 20% DEA in a bubble column to purify a biogas of composition 52% CH_4 and 48% CO_2 into biomethane >95% CH_4 and <5% CO_2, albeit the bubble column requires much lower gas flow rate than packed columns to achieve said results. The study review of Abdeen et al., 2016 concluded that amine scrubbing is more suited for biogas upgrading but requires more research to overcome energy loss and solvent degradation for large scaled applications.

Aside from the simpler semi-empirical models, assumed for vacuum/low pressure or very high temperature operations, for gases, and when there are very small interactions (or interactions that cancel each other) in liquids, most thermodynamic models can be divided into two categoric approaches: $\varphi - \varphi$ models that employ the same EOS to calculate fugacity coefficients in both liquid and vapor phases, thereby ensuring a consistent description, and $\gamma - \phi$ models where the liquid phase is calculated by an activity coefficient model, while the vapor phase utilizes the equation of state to predict its non-ideality.

In oil and gas operations, equation of state (ϕ–ϕ approach) models prove useful in modeling hydrocarbon systems. They can be applied across a broad temperature and pressure range, including subcritical and supercritical regions, and even to mixtures involving diverse components such as light gases and heavy liquids (Kontogeorgis and Gani, 2004). This approach avoids questions of standard states and necessitates only minimal component data to compute thermodynamic properties for the two phases. The PR and Soave – Redlich – Kwong, SRK, equations of state are particularly well-suited to this purpose. Thermodynamic simulation of gas mixtures and brines conducted by Ziabakhsh-Ganji and Kooi (2012) employed PR-EOS, along with random mixing rules, to study the impact of impurities on underground CO_2 storage. Nevertheless, the application of cubic EOS has proven ineffective in numerous instances, particularly when relying on standard rules for mixing and component interaction, that involve multiphase equilibria and highly non-ideal chemical systems. Poormohammadian et al., 2015 reports an extension of the traditional van der Waals one-fluid mixing rule by adding a non-random mixing interaction capable of evaluating the effect of polarity and asymmetry between components present in the system. Harandi et al., 2021 modeled the CO_2 – MDEA – H_2O vapor-liquid equilibrium using five different alpha functions for the Peng – Robinson EOS with Wong – Sandler mixing rule and NRTL activity model by excess Gibbs energy, obtaining a pressure absolute average deviation from experimental data of 18.36%.

It is important to analyze how thermodynamic models are constructed before assuming their reported optimized parameters are accurate representations of the physical phenomena they intend to represent. It is a common occurrence for authors to model complex systems, like the ternary CO_2 – MDEA – H_2O system, while omitting or using literature parameters for the same model application regarding its binary, CO_2 – H_2O, MDEA – H_2O and CO_2 – MDEA systems. There are also discrepancies regarding pure component parameters, such as UNIQUAC volume parameter, r, and surface area parameter, q. Although these parameters should represent a physical property of a given component, the following table displays the inconsistency of their values for similar applications.

Table 1. UNIQUAC volume parameter (r) and surface parameters (q) from different authors.

Reference	r_{MDEA}	q_{MDEA}	r_{CO_2}	q_{CO_2}
Sadegh (2015)	0.13445	0.54315	0.75	2.45
Al-Rashed (2012)	4.2624	3.42	0.92	1.4
Faramarzi* (2009)	1.67	1.56	5.741	6.0806
Prausnitz (1975)	–	–	1.3	1.12
* = CO_2 parameters obtained from Thomsen et al., 1999.				

As stated, Sadegh et al., 2015, reported a calculated volume and surface area parameters of MDEA lower than that of CO_2, which shouldn't be accurate considering MDEA's molecular structure being larger than CO_2. Al-Rashed et al., 2012, used values for r_{CO_2} and q_{CO_2} reported for water by Prausnitz, 1975, even though he reported it to be different for CO_2 as can be observed. Faramarzi et al., 2009, also reported lower size parameters for MDEA compared to CO_2, where the reference of Thomsen et al., 1999, reports r_{CO_2} and q_{CO_2} much higher than what he used for water (Prausnitz parameters). Sandler et al, 2017, proposed a group contribution method, where a molecule is considered to be a collection of functional groups where their size parameters summation would give an accurate approximation of the whole structure. Although this group contribution method reports different water size parameters than Prausnitz, 1975, it follows a logic structure that normalizes molecules used by this method.

4. Theoretical Foundation

4.1 Equation of State – Classic Peng-Robinson

Real gases differentiate from ideal gases by the influence of intermolecular interactions, attractive and repulsive, on its volumetric behavior. For this matter, it is common to apply an adequate equation of state (EOS) capable of describing said overall behavior. Therefore, for the purpose of this work, the classic Peng-Robinson equation of state (Peng et al., 1976) was chosen.

$$P = \frac{RT}{v - b} - \frac{a(T)}{v(v + b) + b(v - b)} \quad \textbf{(1)}$$

where P is the mixture molar pressure, v is the fluid molar volume, R is the universal gas constant and T is the absolute temperature. The energy parameter, a, and the covolume parameter, b, can be expressed at the critical point as:

$$a = 0.45724 \frac{R^2 T_c^2}{P_c} \alpha(T); \;\; b = 0.0778 \frac{RT_c}{P_c} \quad \textbf{(2)}$$

where α is a dimensionless function of reduced temperature, T_r, and acentric factor, ω, which corrects for temperatures other than the critical. There are several alpha (α) functions that were developed throughout the years, such as, Mathias and Copeman et al., 1983, Trebble and Bishnoi et al., 1987, Twu et al., 1995, and Coquelet et al., 1995, but the classical form can be described as:

$$\alpha(T) = \left[1 + m\left(1 - \sqrt{T_r}\right)\right]^2 ; \;\; T_r = \frac{T}{T_c} \quad \textbf{(3)}$$

$$m = 0.37464 + 1.54226\omega - 0.26992\omega^2 \quad \textbf{(4)}$$

where ω represents the acentric factor, which is zero for monoatomic fluids of spheric geometry, growing positive in magnitude as far as the molecular structure deviates from this spheric structural symmetry.

Equation 1 can be rewritten to determine the molar volume of the saturated liquid and vapor phases by substituting the molar volume with the compressibility factor, Z. As such, the EOS turns into a cubic polynomial function, which yields three roots whenever the operating temperature is lower than the critical temperature of the

component. If we analyze the physical significance of these root values, the highest root is associated with the saturated vapor compressibility factor, Z^v, the lowest root with the saturated liquid compressibility factor, Z^l, and the intermediary root has no physical significance as is associated with an unstable equilibrium condition (Z^*).

$$Z^3 - (1-B)Z^2 + (A - 3B^2 - 2B)Z - (AB - B^2 - B^3) = 0 \quad \textbf{(5)}$$

where:

$$A = \frac{aP}{R^2T^2}\ ; \quad B = \frac{bP}{RT}\ ; \quad Z = \frac{Pv}{RT} \quad \textbf{(6)}$$

These equations are valid only for pure components, but can be modified to predict the components behavior inside a mixture, with the addition of a binary interaction parameter k_{ij}, resulting in the following relations.

$$P_{mix} = \frac{RT}{v_{mix} - b_{mix}} - \frac{a_{mix}\alpha(T)}{v_{mix}(v_{mix} + b_{mix}) + b_{mix}(v_{mix} - b_{mix})} \quad \textbf{(7)}$$

$$a_{mix} = \sum_{i=1}^{n}\sum_{j=1}^{n} y_i y_j a_{ij}\ ;\ \ a_{ij} = \sqrt{a_i a_j}\left(1 - k_{ij}\right)\ ;\ b_{mix} = \sum_{i=1}^{n} y_i b_i \quad \textbf{(8)}$$

$$a_i = 0.45724\frac{R^2T_{c,i}^2}{P_{c,i}}\alpha_i(T);\ \ b_i = 0.0778\frac{RT_{c,i}}{P_{c,i}} \quad \textbf{(9)}$$

$$\alpha_i(T) = \left[1 + m_i\left(1 - \sqrt{T_r}\right)\right]^2\ ;\ \ T_{r,i} = \frac{T}{T_{c,i}} \quad \textbf{(10)}$$

$$m_i = 0.37464 + 1.54226\omega_i - 0.26992\omega_i^2 \quad \textbf{(11)}$$

where 'n' is the number of components, v_{mix} is the mixture molar volume, and k_{ij} can be considered zero whenever the molecules in the binary pair have similar size and chemical nature, otherwise they can be determined using approximation models compared to experimental data.

These binary interaction parameters can be found by fitting the equation of state to vapor – liquid equilibrium mixture data, and the combining rules of Equation 8 are referred to as the van der Waals one-fluid mixing rules, since both the mixture and the

pure fluids are being described by the same equation of state, albeit the mixture becomes concentration dependent.

4.2 Fugacity coefficient and Fugacity

In the presence of intermolecular interactions, exerted pressure is no longer equal to its pressure value calculated by the EOS, on the basis that said interactions will deviate from the ideal behavior. As such, the corrected pressure is called fugacity and can be described as follows.

$$f^v = \varphi^v . P \rightarrow \varphi^v = \frac{f^v}{P} \quad \textbf{(12)}$$

$$\lim_{P \to 0} \varphi^v = 1 \rightarrow \lim_{P \to 0} f^v = 0 \quad \textbf{(13)}$$

where φ^v is the correction factor of pressure, called fugacity coefficient, and f^v is the fugacity. Therefore, the fugacity coefficient measures how far the real gas moves away from the ideal behavior, and tends to unity when the pressure tends to zero, at which limit the effects of intermolecular interactions initially present will not be perceptible.

Outside the limits from Equation 13, there are two possible scenarios: predominance of repulsive interactions, in which case, there is an increase in the exerted pressure in relation to the ideal gas resulting in a fugacity coefficient higher than unity, and predominance of attractive interactions, where the opposite occurs and fugacity coefficient is a positive number between zero and one. In this sense, the fugacity coefficient becomes useful for pure fluids chemical potential calculations based on knowledge of the molar Gibbs energy of an ideal gas. The fundamental relations for molar Gibbs energy of an ideal and real gases makes it so that they become a function solely based on temperature and pressure of the gas.

$$dg^{*,v} = -s^{*,v} . dT + v^{*,v} . dP \quad \textbf{(14)}$$

where the superscript "*" relates to a reference state, which in this case, is the ideal pure gas, and the "v" superscript relates to real vapor phase behavior. If the temperature is fixed, and correlating pressure to fugacity for real gas as described in Equation 12, the following equations.

$$dg^*)_T = v^*.dP = \frac{R.T}{P}.dP = R.T.dlnP \quad \textbf{(15)}$$

$$dg^v)_T = v^v.dP = R.T.dlnf^v \quad \textbf{(16)}$$

$$d(g^v - g^*) = \left(v^v - \frac{R.T}{P}\right).dP = R.T.dln\left(\frac{f^v}{P}\right) = R.T.ln\varphi^v \quad \textbf{(17)}$$

By integrating Equation 17 from its ideal gas limit to its real gas limit, we get the following relations.

$$\int_0^{g^v - g^*} d(g^v - g^*) = \int_{P\to 0}^{P} \left(v^v - \frac{R.T}{P}\right).dP = R.T \int_0^{ln\varphi^v} dln\varphi^v \quad \textbf{(18)}$$

$$g^v - g^* = R.T.ln\varphi^v = \int_{P\to 0}^{P} \left(v^v - \frac{R.T}{P}\right).dP \quad \textbf{(19)}$$

Therefore, if the fugacity coefficient is known, the molar Gibbs energy of the real pure gas, in other words, its chemical potential, can be calculated from the value in absence of interaction between molecules. The calculation of said fugacity coefficient can also be used for the liquid phase, and requires the usage of a volumetric EOS explicit in molar volume, $v^{v,l}(T,P)$.

$$g^{v,l}(T,P) = g^*(T,P) + RTln\varphi^{v,l} \quad \textbf{(20)}$$

$$ln\varphi^{v,l} = \int_{P\to 0}^{P} \left(\frac{v^{v,l}}{RT} - \frac{1}{P}\right).dP \quad \textbf{(21)}$$

Usually, fluid volumetric equations of state are explicit in pressure, which requires a slight alteration in the integral variable from v to P. Applying Equation 6 for the compressibility factor, we arrive at the function capable of calculating fugacity coefficient with the corresponding molar volume EOS.

$$\int_{P\to 0}^{P} \left(\frac{v^{v,l}}{RT} - \frac{1}{P}\right).dP = Z - 1 - \ln Z - \int_{v\to\infty}^{v} \frac{P}{R.T} - \frac{1}{v}.dv \quad \textbf{(22)}$$

Finally, by inserting Equation 21 into 22, and considering the Peng-Robinson EOS, the characteristic function used into the thermodynamic model can be written as follows.

$$\ln \varphi^{v,l} = Z^{v,l} - 1 - \ln Z^{v,l} - B - \frac{A}{2\sqrt{2}} \ln \left(\frac{Z^{v,l} + \left(1 + \sqrt{2}\right).B}{Z^{v,l} + \left(1 - \sqrt{2}\right).B} \right) \quad \textbf{(23)}$$

Therefore, by solving Equation 5, it is possible to arrive at the fugacity coefficient for both vapor and liquid phase of a system in a determined temperature and pressure.

4.3 Real mixture: φ – φ approach

The calculations for vapor-liquid equilibrium involving real mixtures requires the development of chemical potential equations capable of accounting for interactions between components in the vapor phase, as well as, asymmetry in sizes, shapes and chemical natures in the liquid phase. Therefore, an analogous procedure to the one previously developed to arrive at Equation 20 can be designed to include the concept of components molar partial volume in our mixture and to establish its connection to the variation of chemical potential and pressure.

This component molar partial volume can be defined as the derivative of the mixture volume in relation to the number of moles of said component, while fixing the temperature, pressure and number of mols of the other components. Since the volume of a mixture can be obtained from deriving Gibbs free energy in relation to the pressure, we can establish the following relations.

$$\bar{v}_i = \left(\frac{\partial V}{\partial n_i} \right)_{T,P,n_j} \quad ; \quad V = \left(\frac{\partial G}{\partial P} \right)_{T,P,\vec{n}} \quad \textbf{(24)}$$

$$\bar{v}_i = \frac{\partial}{\partial n_i} \left(\frac{\partial G}{\partial P} \right) = \frac{\partial}{\partial P} \left(\frac{\partial G}{\partial n_i} \right) = \left(\frac{\partial \mu_i}{\partial P} \right)_{T,\vec{x}} \quad \textbf{(25)}$$

$$d\mu_i)_{T,\vec{x}} = \bar{v}_i dP \quad \textbf{(26)}$$

Therefore, the partial volume of any component measures how sensitive its chemical potential is in relation to system pressure. As a starting point, Equation 26 can be used for a mixture of ideal gases, which gives the following.

$$d\mu_i^*)_{T,\vec{y}} = R.T.dln(y_i.P) = R.T.dlnP = \frac{R.T}{P} dP \quad \textbf{(27)}$$

Since the chemical composition of the gas is fixed, for a mixture of ideal gases we have:

$$d\mu_i^*)_{T,\vec{y}} = R.T.dlnP_i \quad \textbf{(28)}$$

Through the effect of fluid characteristic intermolecular interactions, the partial pressure must be replaced by the fugacity of the component in the mixture, which can be defined analogously to the definition used in the field of thermodynamics applied to pure fluids of Equation 12:

$$\hat{f}_i^v = \hat{\varphi}_i^v . P_i \quad \textbf{(29)}$$

$$\lim_{P\to 0} \hat{f}_i^v = \lim_{v\to\infty} \hat{f}_i^v = P_i \quad \rightarrow \quad \lim_{P\to 0} \hat{\varphi}_i^v = \lim_{v\to\infty} \hat{\varphi}_i^v = 1 \quad \textbf{(30)}$$

where, $\hat{\varphi}_i^v$, represents the fugacity coefficient of the *ith* component in the mixture, being the partial pressure correction factor for the effect of intermolecular interactions. On the limit in which the mixture behaves as ideal (pressure tending to zero or volume tending to infinity) the fugacity becomes identical to the partial pressure of the component.

Following the same train of thought of Equation 14 to 21 we arrive at similar equation for fugacity coefficient of each component in relation to the selected EOS.

$$ln\hat{\varphi}_i^v = \int_{P\to 0}^{P} \left(\frac{\bar{v}_i^v}{RT} - \frac{1}{P}\right).dP \quad \textbf{(31)}$$

Similarly, as was explained in its pure component counterpart, fluid volumetric equations of state are explicit in pressure, which requires a slight alteration in the integral variable from v to P.

$$ln\hat{\varphi}_i^v = -\left(\ln Z^v + \int_{v\to\infty}^{v^v} \left[\frac{1}{R.T}.\frac{\partial P}{\partial n_i}\right)_{T,v,n_{j\neq i}} - \frac{1}{v}\right] dv\right) \quad \textbf{(32)}$$

It should be noted that the implementation of the above equation requires knowledge of the molar volume and vapor phase compressibility factor, both properties resulting from the resolution of the volumetric EOS chosen for the fluid of interest, which must be extended to take into account the effect of chemical composition. This

task is carried out by introducing mixing rules, which, in general terms, determine how the chemical composition of the mixture affects the values of the characteristic parameters of the mixture equation. One such example is the binary interaction parameter, k_{ij}, explained in Equation 8.

Symmetric equations can be used to calculate chemical potentials in a real liquid mixture, being the molar volume and phase compressibility factor also resulting from the resolution of the EOS representative of the fluid fixing T, P and the overall composition of the mixture. The vapor – liquid equilibrium can be determined as follows.

$$\hat{f}_i^v = \hat{f}_i^l \tag{33}$$

$$\hat{f}_i^v = y_i \varphi_i^v P \quad ; \quad \hat{f}_i^l = x_i \varphi_i^l P \tag{34}$$

This method of evaluating the behavior of vapor and liquid phases only with concepts of fugacity coefficient at equilibrium is called the φ – φ method. When we apply the classic Peng – Robinson EOS, the fugacity coefficient of each component can be obtained as follows.

$$\ln \varphi_i^{v,l} = \frac{b_i}{b}(Z^{v,l} - 1) - \ln(Z^{v,l} - B) + \frac{A}{B.2\sqrt{2}}\left(\left(2\sum_{j=1}^{N} x_j a_{ij}\right)\Big/ a - \frac{b_i}{b}\right)\ln\left(\frac{Z^{v,l} + (1-\sqrt{2})B}{Z^{v,l} + (1+\sqrt{2})B}\right) \tag{35}$$

In this works present algorithm, there is a need to initially guess the systems pressure, which may result in some discrepancies in the equality of Equation 33, caused by inaccuracies in the EOS ability to predict $\varphi_i^{v,l}$.

It becomes possible to establish a generic vapor pressure calculation algorithm for real fluids as a function of temperature based on the thermodynamic knowledge developed in Equation 23. This type of algorithm has been called as “reactive bubble pressure algorithm” by Harandi et al., 2021, however, since the authors don’t elaborate on their convergence criterion, this work developed the following methodology.

4.3.1 Pure Component Systems

For the calculation of pure component systems, we establish an initial guess for the saturated pressure, followed by the calculation of the EOS interaction parameters and root solution of its cubic form as described in the previous sections. After obtaining the fugacity coefficients of each phase with Equation 35, at equilibrium, molar Gibbs energy in each phase should be equal, and so should be their fugacity coefficients. This fact allows the definition of our first convergence criterion.

$$\left|\frac{\varphi^l}{\varphi^v} - 1\right| < \varepsilon \tag{36}$$

where ε, is the defined tolerance of convergence, usually a number in an order of magnitude lesser than 10^{-5} that if reached, the pressure is found. If the convergence criterion isn't reached, a new guess for pressure must be updated at the first step in accordance to the following relation based on Equation 21.

$$P_1 = P_0 . \left(\frac{\varphi_i^l}{\varphi_i^v}\right) \tag{37}$$

$$\left[\frac{v_i^l - v_i^v}{R.T}\right] = \frac{dln\left(f_i^l / f_i^v\right)}{dP} = \frac{\partial ln\left(\varphi_i^l / \varphi_i^v\right)}{\partial P}\Bigg)_T < 0 \tag{38}$$

At a fixed temperature, the derivative of Equation 38 will always be negative, since liquid molar volume is lower than vapor molar volume. Therefore, the physics principle behind the convergence criterion logic of Equation 37 can be understood as follows: if the ratio is higher than one, the pressure needs to increase in order to lower that ratio, if it is lower than one, the opposite is true. This strategy is useful to predict saturated pressure of pure components, and is an important part of this works optimization algorithm for the acentric factor.

4.3.2 Multicomponent Systems

The second convergence criterion pertains to the equality of Equation 33, in which the partial Gibbs free energy of both phases should be equal. An initial guess for the composition of the system at the corresponding initial guess of pressure and fixed temperature needs to be set as to allow the calculation of said Gibbs free energy. As such, we can establish the following relations:

$$K_i = \frac{x_i \varphi_i^l}{y_i \varphi_i^v} \rightarrow (K_i - 1)^2 < \varepsilon_i \quad \textbf{(39)}$$

where, K_i, is a constant that should be equal to unity at equilibrium, and ε_i, is another defined tolerance of convergence for each component, usually a number in an order of magnitude lesser than 10^{-5} that if reached, the vapor – liquid equilibrium is found. Instead of getting the absolute value of the difference $K_i - 1$, we decided to raise its square value to increase the speed of the algorithm.

The logic behind Equation 39 loop of convergence is as follows: if the defined tolerance, ε_i, isn't reached for all components present in the system, then the initial guess of composition should be updated as follows:

$$y_{i,1} = y_{i,0}.K_i \quad \textbf{(40)}$$

Since the only update to the algorithm is the composition of the vapor phase, the components vapor fugacity coefficient are recalculated using the new values. However, after achieving the defined tolerance for all components in the mixture, the composition, y, tends to be higher than unity, a physics incongruency, since the initial pressure used was a guess value. As such, there is a need for a second loop inside the algorithm.

$$y = \sum_{i=1}^{N} y_i \quad \therefore \quad |y - 1| \geq \varepsilon' \rightarrow P_1 = P_0.y \quad \textbf{(41)}$$

The new pressure will then be used to recalculate the fugacity coefficient of both phases, restarting the loop described in Equation 39. This condition creates a pressure calculation outer loop after the initial composition loop.

4.4 Real mixture: γ – φ approach

There are situations where it is not possible to find an EOS capable of describing the volumetric properties of the fluid's liquid state. This usually occurs when, in the fluid, coexist molecules with significant differences in shape, size and chemistry nature. In this way, in order to extend the formalism of classic thermodynamics to these situations it becomes necessary to find a way to calculate the

chemical potential of components in the liquid phase without the need for evaluation of fugacity coefficients. For this, the concept of chemical activity must be introduced, which can be understood as the ratio between the fugacity of the component in the mixture divided by the fugacity of the same component in some reference state.

$$a_i = \frac{\hat{f}_i}{f_i^+} \tag{42}$$

where, a_i, is the component's chemical activity, $\hat{f}_i$, is the component's fugacity in the mixture and f_i^+, is the same component's fugacity in the defined set of standard conditions. As such, the chemical potential of any component in a liquid mixture can be calculated by expanding on Equations 20, 26 and 27:

$$\int_0^{\mu_i^l - \mu_i^*} d\left(\mu_i^l - \mu_i^*\right) = \int_{P\to 0}^{P} \left(\bar{v}_i^l - \frac{R.T}{P}\right).dP = R.T \int_0^{\ln \hat{\varphi}_i^l} d\ln \hat{\varphi}_i^l \tag{43}$$

$$\mu_i^l = \mu_i^* + R.T.\ln \hat{\varphi}_i^l \quad \therefore \quad \mu_i^* = g_i^* + RT\ln x_i \tag{45}$$

$$\mu_i^l(T,P,\vec{x}) = g_i^l(T,P) + RT\ln\left(\frac{x_i.\hat{\varphi}_i^l}{\varphi^l}\right) \tag{46}$$

Taking into consideration that the mixture's pressure is equal to the pressure of the reference state (pure component), it is possible to manipulate Equation 46 to calculate the chemical potential of the liquid phase based on Equation 42:

$$\mu_i^l = g_i^l + RT\ln\left(\frac{x_i.P.\hat{\varphi}_i^l}{P.\varphi^l}\right) = g_i^l + RT\ln\left(\frac{\hat{f}_i^l}{f_i^l}\right) = g_i^l + RT\ln a_i^l \tag{47}$$

$$a_i^l = x_i.\left(\frac{\hat{\varphi}_i^l}{\varphi_i^l}\right) \tag{48}$$

where, a_i^l, represents the chemical activity of a component in the mixture, being directly related with the ratio between fugacity coefficient in the mixture and as a pure component. This ratio of fugacity coefficients is called chemical activity coefficient, $\hat{\gamma}_i^l$.

$$\hat{\gamma}_i^l = \frac{\hat{\varphi}_i^l}{\varphi_i^l} \quad \therefore \quad a_i^l = x_i.\hat{\gamma}_i^l \tag{49}$$

Chemical activity coefficients can be determined from functions known as excess Gibbs energy (G_{ex}^{l}). In this work the Universal Quasi-Chemical model, UNIQUAC, is going to be used to calculate the excess Gibbs energy.

$$G_{ex}^{l}(T, P, \vec{n}) = RT \sum_{i} n_i \ln \hat{\gamma}_i^{l} \quad \textbf{(50)}$$

The UNIQUAC model treats the mixture as a set of distributed molecules in an incompressible lattice of coordination number equal to Z (number of first neighbors with respect to a given central atom, varying between 8 and 10 for liquids), where each molecule is described by a representative parameter of its contact area (q_i) and "size" (r_i), the latter being the number of constituent segments of the molecule. In this way, two fractions can be defined for each component, its volume fraction ($\emptyset_i$) and its fraction of area (θ_i), both defined below (Prausnitz et al., 1975).

$$\emptyset_i = \frac{x_i . r_i}{\sum_i x_i . r_i} \quad \textbf{(51)}$$

$$\theta_i = \frac{x_i . q_i}{\sum_i x_i . q_i} \quad \textbf{(52)}$$

These dimensional parameters are going to be evaluated based on the group contribution method of Prausnitz, in which a molecule can be determined to be a collection of functional groups, each with its own r_i and q_i. As such, in this work, these parameters are going to be determined based on the values reported by professor J. Gmehling of the University of Oldenburg, Germany, presented at Sandler's "Chemical, Biochemical, and Engineering Thermodynamics fifth edition". As reported in the literature review of Sadegh et al., 2015, there isn't a defined consensus for these parameters, and by using the group contribution method, we intend to avert possible errors.

The excess Gibbs energy in the UNIQUAC approach also involves the effect of binary interactions between different components. This effect is captured by the parameter τ_{ij} of each binary, which is related to the potential energies of interaction between ij pairs (u_{ij}) and ii pairs (u_{ii}), with i and j varying among all components present in the system.

$$\tau_{ij} = \exp\left(\frac{-w_{ij}}{T}\right) \quad ; \quad w_{ij} = w_{ij}^{0} + w_{ij}^{T}(T - 298.15) \quad ; \quad w_{ij} = u_{ij} - u_{jj} \qquad \textbf{(53)}$$

where T is the temperature of the system and w_{ij}^{0} and w_{ij}^{T} are the UNIQUAC adjustable interaction parameters assumed to be temperature dependent.

In the expression for G_{ex} the effect of the shape and size of the molecules is concentrated in the term described as combinatorial, while the effect of intermolecular interactions in the residual term. Note that area fractions appear in both terms, because the area of a given molecule affects the ability to allocate it in the network (combinatorial term), as well as how available it is to interact (residual term).

It is possible to contemplate the equations for both contributions mentioned in a format suitable for multi-component blends.

$$\frac{G_{ex}(combinatorial)}{RT} = \sum_i x_i \ln\frac{\phi_i}{x_i} + \frac{Z}{2}\sum_i x_i q_i \ln\frac{\theta_i}{\phi_i} \qquad \textbf{(54)}$$

$$\frac{G_{ex}(residual)}{RT} = -\sum_i q_i x_i \ln\left(\sum_j \theta_j \tau_{ji}\right) \qquad \textbf{(55)}$$

Of course, as expected, the model for calculating the activity coefficient chemistry of any component will also involve two contributions, one being from combinatorial nature and the other residual, the first associated with the effect of shape and size of molecules and the second determined by the nature of the binary interactions present.

$$\ln\gamma_i = \ln\gamma_i(combinatorial) + \ln\gamma_i(residual) \qquad \textbf{(56)}$$

$$l_i = \frac{Z}{2}(r_i - q_i) - (r_i - 1) \qquad \textbf{(57)}$$

$$\ln\gamma_i(combinatorial) = \ln\frac{\phi_i}{x_i} - \frac{Z.q_i}{2}\ln\frac{\phi_i}{\theta_i} + l_i - \frac{\phi_i}{x_i}\sum_j x_j l_j \qquad \textbf{(58)}$$

$$\ln \gamma_i(residual) = q_i \left[1 - \ln\left(\sum_j \theta_j \tau_{ji} \right) - \sum_j \frac{\theta_j \tau_{ij}}{\sum_k \theta_k \tau_{kj}} \right] \quad \textbf{(59)}$$

In this work, the binary interaction parameters pertaining the potential energy of interaction, u_{ij}, are going to be optimized to allow for accurate and scalable predictions of systems pressure following a similar methodology applied to the φ – φ approach. The optimization of acentric factor for pure components should follow the same methodology as the one presented for the φ – φ method, since in this case, there is no difference in shape, size and chemical nature of present molecules in the system.

However, for multicomponent systems, there is need for a slight alteration regarding the presence of activity coefficient for the liquid phase. Analogous to the previous model, an initial guess of pressure and composition is set into the algorithm, which will be used to predict the vapor – liquid equilibrium similarly to Equation 36, with the corresponding substitution of activity coefficient for the liquid phase.

$$K_i = \frac{x_i . \gamma_i^l . P_i^{sat}}{y_i . \varphi_i^v . P} \rightarrow (K_i - 1)^2 < \varepsilon_i \quad \textbf{(60)}$$

where, P_i^{sat}, is the saturated pressure, γ_i^l, is the activity coefficient and φ_i^v, is the fugacity coefficient of each component. The defined tolerance, ε_i, should also be a number of lower magnitude than 10^{-5}.

The logic for convergence follows the exact same methodology as the one described by Equations 40 and 41 of the φ – φ method.

4.5 Empirical "Non – random" mixing rule

The empirical "non-random" mixing rule aims to overcome the difficulty of binary interaction parameter, k_{ij}, to describe system interaction with polar and asymmetric compounds. The chemical nature of these systems develops regions of non-uniform distribution at the molecular level, which should be accounted for when calculating the EOS energy parameters (Poormohammadian et al., 2015), as described below.

$$a = a^C + a^A \tag{60}$$

$$a^A = \sum_i \sum_j -l_{ij}(x_i - x_j)x_i x_j (a_i a_j)^{1/2} \quad ; \quad l_{ij} = -l_{ji} \tag{60}$$

where a^A is the asymmetric term due to polarity, l_{ij} is the binary interaction coefficient for the asymmetric term and a^C is the conventional random mixing term described in Equation 8.

4.6 Wong – Sandler mixing rule

As was explained in section 2.1, the van der Waals one-fluid mixing rule is used in this work to describe the components interaction effect in the classic Peng – Robinson's equation of state's parameters. However, the simplicity of this mixing rule may not be appropriate whenever the underlining system deviates considerably from the ideal behavior.

To try and solve this issue, the Wong – Sandler mixing rule was proposed as the combination of an equation of state and excess Gibbs energy, allowing simple EOS to describe all mixtures. Since, in this work, we intend to predict the liquid – vapor equilibrium of binary systems involving CO_2, which has a low critical temperature and form a highly nonideal CO_2 – H_2O binary system, this mixing rule shows enough potential to improve on our classic Peng – Robinson thermodynamic model.

It is described in Wong et al., 1992, that through the analysis of the second virial coefficient of any cubic EOS, it is feasible to arrive at the following relations for calculating the interaction parameters of said EOS.

$$a = b\left[\frac{G_{ex}}{C^*} + \sum_i \frac{x_i a_i}{b_i}\right] \quad ; \quad b = \frac{\sum_i \sum_j x_i x_j \left(b - \frac{a}{RT}\right)_{ij}}{1 - \frac{F(x)}{RT}} \tag{61}$$

$$F(x) = \frac{G_{ex}}{C^*} + \sum_i x_i \frac{a_i}{b_i} \tag{62}$$

$$\left(b-\frac{a}{RT}\right)_{ij}=\frac{\left(b-\frac{a}{RT}\right)_{i}+\left(b-\frac{a}{RT}\right)_{j}}{2}\left(1-k_{ij}\right) \quad \textbf{(63)}$$

where G_{ex} denotes the excess Gibbs energy that will be obtained using the UNIQUAC model, C^{*} is a constant whose value depends upon the EOS used, being equal to -0.62323 for Peng – Robinson, k_{ij} is the binary interaction parameter and $F(x)$ is a function of composition.

4.7 Overall thermodynamic methodology

This work's proposed algorithm is our take in the so-called "reactive bubble pressure algorithm", starting from lower complexity of pure component systems, and incrementally optimizing model parameters whenever there is an increase in complexity towards binary and multicomponent systems. In this section, a step-by-step procedure, as well as, the reasoning behind the initial guesses used, are described.

As such, to corroborate the accuracy of the optimized parameters, the predicted pressure and compositions are compared with experimental data and evaluated based on the absolute relative average deviation, ARD%, of each dataset. For the pure component systems, the objective function minimized by the "fminsearch" MATLAB's function, based on the predicted pressure obtained from guesses of the acentric factor, ω, and can be described as follows:

$$ObjectiveFunction=\sum\left|\frac{P_{cal}-P_{exp}}{P_{cal}}\right| \quad \textbf{(64)}$$

The logic behind the "fminsearch" function is to arrive at an objective function local minimum value by altering the argument value of its supplied model parameter. Since it obtains a local minimum, it is recommended to run this function with multiple different initial guesses, on the possibility that there is a global minimum lower than your initial guesses local minimum. If multiple arguments converge to the same value, it is possible to assume that it is a global minimum for that application. A modelling flowchart for the optimization of acentric factor is described in Figure 1.

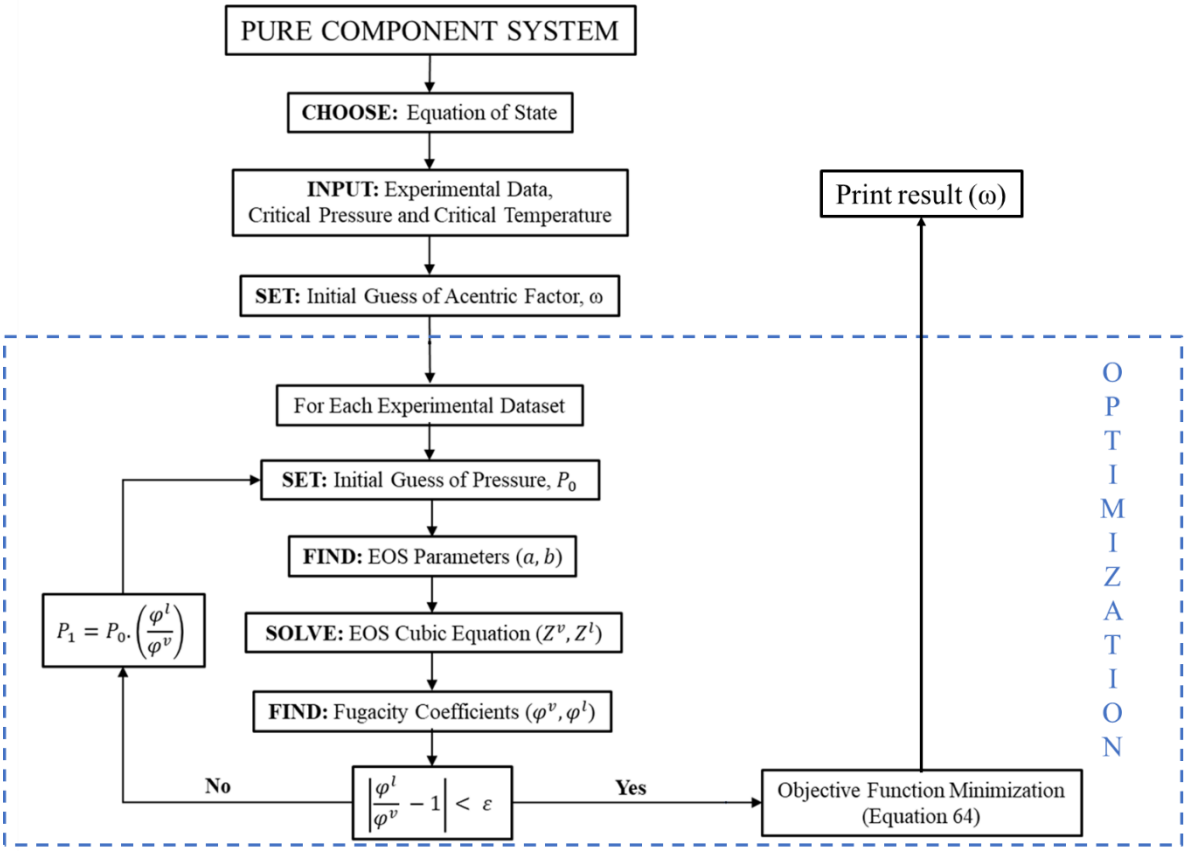

Figure 1. Pure component modelling flowchart for acentric factor optimization.

The sequential steps for pure components systems saturated pressure calculations can be described as follows:

1) Choose an equation of state capable of predicting the behavior or real gases, preferably one that has a well-defined polynomial form with thermodynamic significant roots, such as this work's classic Peng – Robinson.
2) Input intrinsic molecular properties necessary for the calculation, in this case, critical pressure, P_c, and critical temperature, T_c, as well as, supplying accurate experimental data corroborated by literature. This experimental data will determine the temperatures at which the algorithm will predict the pressure.
3) Set an initial guess for the acentric factor, ω, which in this work, was considered to be equal to the literature values for each component (Harandi et al., 2021). The following steps 4 – 8 are optimized inside the objective function minimization procedure described in Equation 64.

4) Set an initial guess for the system pressure, P_0, which is used in the EOS's cubic form of as described by Equation 6.
    a. In this work, the experimental data's temperature range was previously sorted in an ascending order. That way, the initial guess of pressure for the first dataset was equal to its experimental data equivalent. After the first predicted pressure is calculated by the model, its value is supplied as the initial guess for the second dataset, as we believe it would give an approximate order of magnitude for that guess.
    b. If the model still find trouble converging in this step, because the experimental data isn't sorted, or the system behaves erratically, it is recommended to always supply the experimental datapoint as the initial guess for pressure.
5) Find the equation of state interaction parameters. In this work, classic Peng – Robinson requires the calculation of energy parameter, a, and covolume parameter, b.
6) Solve the cubic EOS form to obtain Z^v and Z^l, reminding that the solution should present three roots when the temperature of the system is lower than the critical temperature of components. The higher value root is the vapor phase, while the lower value root is the liquid phase.
7) Find the fugacity coefficients φ^v and φ^l using Equation 32 adapted to the selected EOS of Step 1.
8) Check if the convergence criterion is achieved, updating the pressure according to Equation 38 in case it hasn't. After the tolerance has been reached, print the value for acentric factor.

For binary systems the flowchart has some modifications regarding the optimized interaction parameter and calculation structures and can be seen bellow.

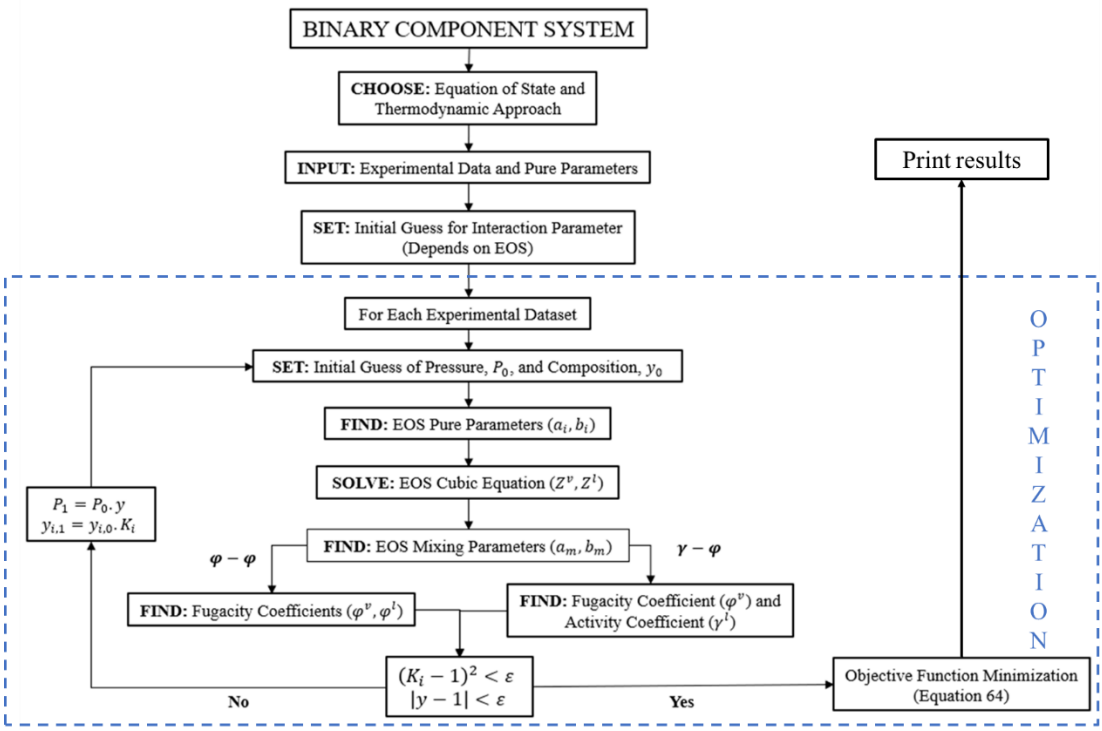

Figure 2. Binary system modelling flowchart for interaction parameters optimization.

The sequential steps for pure components systems saturated pressure calculations can be described as follows:

1) Choose an equation of state and thermodynamic approach ($\varphi - \varphi \; or \; \gamma - \varphi$).
2) Input pure component parameters such as critical pressure, P_c, critical temperature, T_c, and acentric factor, ω, as well as, supplying accurate experimental data corroborated by literature. This experimental data will determine the temperatures at which the algorithm will predict the pressure.
3) Set an initial guess for the interaction parameters according to the selected EOS and mixture rule. In this work, it is the interaction parameters, k_{ij} and l_{ij} for the classic Peng – Robinson with non-random mixing rule and UNIQUAC parameters $u_{12}^0, u_{12}^T, u_{21}^0, u_{21}^T$ for the Wong – Sandler mixing rule. The following steps 4 – 8 are optimized inside the objective function minimization procedure described in Equation 64.
4) Set an initial guess for the system pressure, P_0 and composition, y_0, which is used in the EOS's cubic form of as described by Equation 6.

a. In this work, the experimental data's temperature range was previously sorted in an ascending order. That way, the initial guess of pressure and composition for the first dataset was equal to its experimental data equivalent. After the first predicted pressure and composition are calculated by the model, their values are supplied as the initial guess for the second dataset, as we believe it would give an approximate order of magnitude for that guess.
b. If the model still find trouble converging in this step, because the experimental data isn't sorted, or the system behaves erratically, it is recommended to always supply the experimental datapoint as the initial guess.

5) Find the equation of state pure parameters. In this work, classic Peng – Robinson requires the calculation of energy parameter, a_i, and covolume parameter, b_i.
6) Solve the cubic EOS form to obtain Z^v and Z^l, following the same logic as previously described.
7) For $\varphi - \varphi$ approach: Find the fugacity coefficients φ^v and φ^l using Equation 32 adapted to the selected EOS of Step 1. For $\gamma - \varphi$ approach: Find the activity coefficient, γ^l using Equation 56, and φ^v using Equation 32 adapted to the selected EOS of Step 1.
8) Check if the convergence criterions are achieved, updating the pressure and composition of the gas phase according to Equation 38 in case it hasn't. After the tolerance has been reached, print the value for the interaction parameters.

5. Results Discussion

5.1 Pure components

As previously stated, this work intends to determine all parameters used in its overall model calculations, as to not allow for potential propagated errors present in the literature to influence its results. The critical properties from the literature, and the experimental data temperature and pressure ranges can be observed in the following table:

Table 2. Critical properties and experimental data ranges for the components.

Component	Critical Temperature (K)	Critical Pressure (MPa)	Acentric Factor (literature)	Experimental Data Temperature Range (K)	Experimental Data Pressure Range (kPa)	Bibliographic Reference
Water	647.3	22.12	0.344	293 – 571	2.4E+00 – 8.37E+03	Dortmund Data Bank
MDEA	677.1	3.70	1.24	293 – 402	6.1E-04 – 1.48E+00	Noll et. al., 1998
CO_2	304.21	7.29	0.224	223 – 298	6.79E+02 – 6.44E+03	Dortmund Data Bank

The vapor-liquid systems were determined sequentially, starting from the least complex ones, the pure components, while moving towards greater complexity, the binary systems. As such, the acentric factor, ω, was calculated for each of the components, and the absolute average deviation, AAD, was compared with their corresponding literature values.

5.1.1 Water

The experimental data for vapor pressure of water was obtained from the Dortmund Data Bank (DDBST) website as shown in the appendix.

The initial guess for pressure was set as the first experimental pressure of 2.400 kPa, and the objective function for calculating the acentric factor was minimized using MATLAB “fminsearch” function. The initial guess value used for the minimization was its literature correspondent.

The optimization resulted in an acentric factor ω = 0.3275, which is a slight alteration to its literature counterpart of ω = 0.344. Both the optimized and literature ω were used to calculate the saturated pressure of 1000 equally distanced temperatures between the lowest and highest experimental values of temperature (K) in Figure 3.

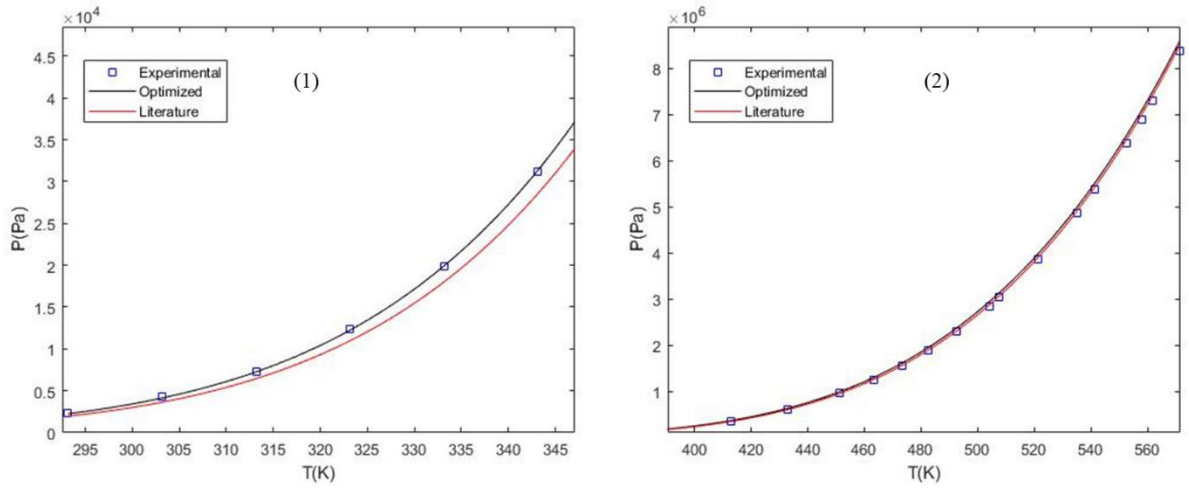

Figure 3. Calculated saturation pressure of water at low temperature (1) and high temperature (2), while using the optimized acentric factor, w = 0.3275 (-), and its literature counterpart, w = 0.344 (-). The experimental data from DDBST was plotted as well (□).

As can be observed, both values agree with the experimental data from DDBST, however, to further understand which deviates more, the absolute relative deviation pressure error of each point, and the absolute average deviation, AAD, were calculated and are shown in Figure 4.

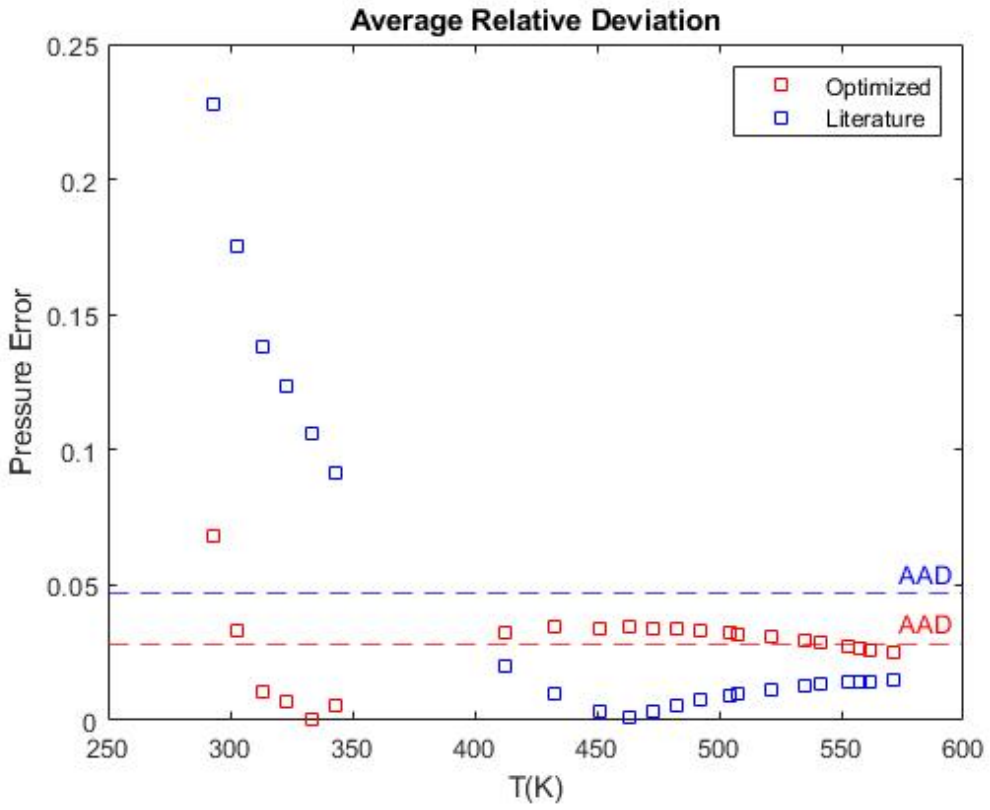

Figure 4. Average relative and absolute deviations of pure water for the optimized (□) and literature (□) values of ω at different temperatures (K).

While the optimized ω resulted in better calculated saturation pressures at lower temperatures, which coincides with the temperature range in which chemical absorption processes in biogas purification occurs, at around 400 K there is a shift towards better results using the literature value. In this sense, the AAD% for the optimized ω was calculated as 2.81% while the literature ω resulted in 4.67%, demonstrating that, overall, the EOS is capable of predicting the saturated pressure across the temperature range, but the optimized ω should be better suited for the thermodynamic model, since the chemical absorption process usually occurs at temperatures lower than 400 K.

5.1.2 MDEA

Following the same methodology used for the water pure component, the initial guess value of ω was the literature value, and the initial pressure guess was the first experimental data of 6.10×10^{-4} kPa value, as described in Table 1.

The optimization resulted in ω = 1.0133, which is fairly different from the literature value of ω = 1.2400. Similarly, to the previous step, these values were used to plot the calculated saturated pressure at different temperatures and compared to its experimental data, as shown in Figure 5.

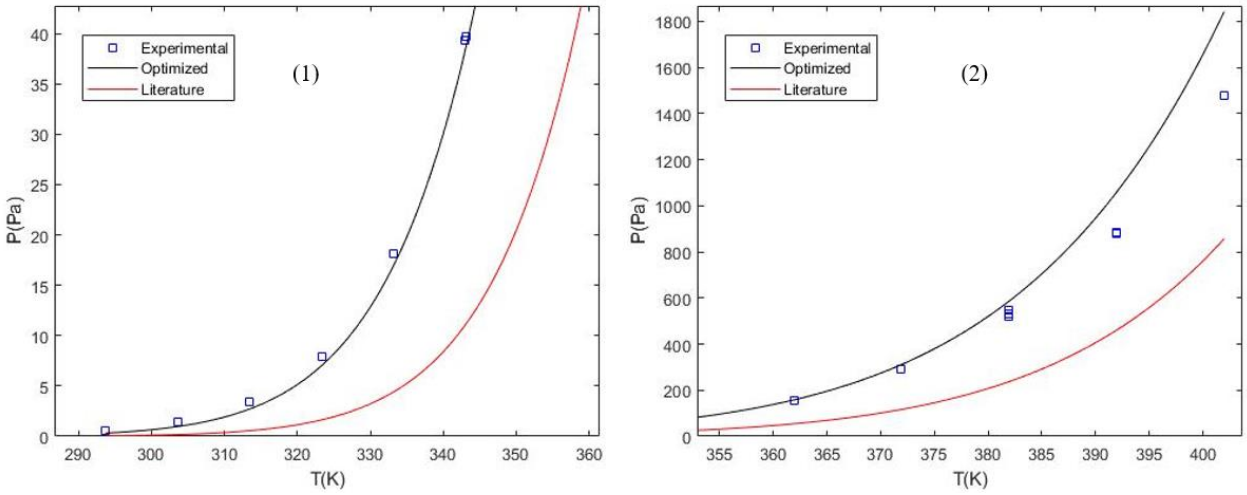

Figure 5. Calculated saturation pressure of MDEA at low temperatures (1) and high temperature (2), while using the optimized acentric factor, w = 1.0133 (-), and its literature counterpart, w = 1.2400 (-). The experimental data from Noll et al., was plotted as well (□).

As can be observed, the literature value is not very well suited to calculate the saturated pressure of MDEA via the classic Peng – Robinson EOS, which decreases its viability when using it for more complex models involving other components. This fact is evident whenever we analyze the pressure errors and its AAD, as shown in Figure 6.

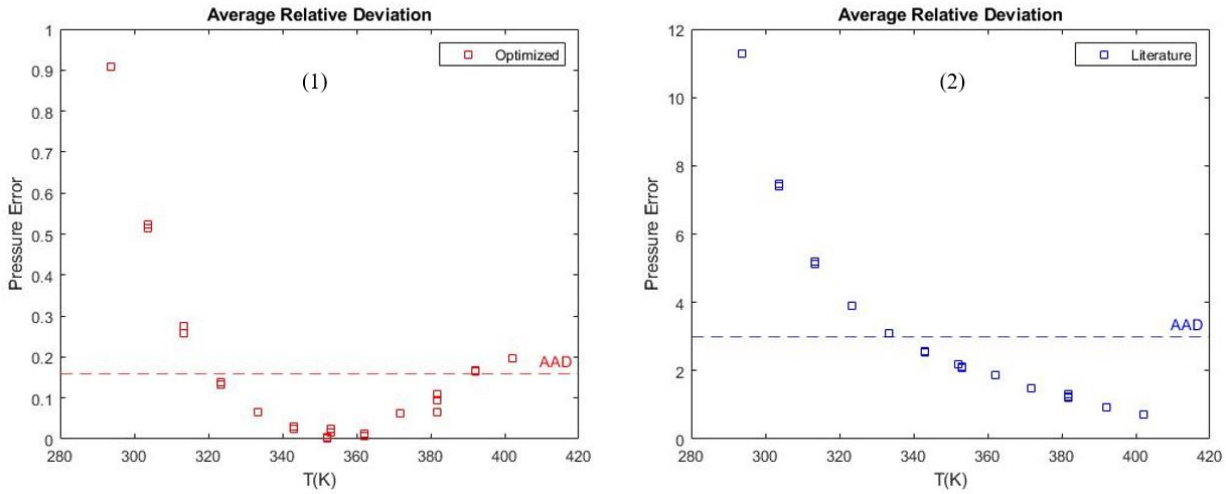

Figure 6. Average absolute deviation of pure MDEA for the optimized (1) and literature (2) values of ω at different temperatures (K).

Opposite to the errors obtained for the water saturated pressure, MDEA agreed with experimental data at higher temperatures inside the analyzed range. This fact could be associated with the increase in polarity of this component at lower temperatures, while PR-EOS being fundamentally and equation of state aimed at modelling apolar systems for petroleum cracking.

Even though the optimized ω is apparently better for calculating the saturated pressure, it still resulted in an AAD% = 15.86, which can be concerning when using the model for binary calculations. However, the literature value expresses an astounding AAD% = 299.61, deviating a lot from experimental data.

The reason for this disparity between model and experimental data could be associated with the capacity of the EOS to accurately calculate the correct saturated pressure. Another reason could be the fact that the experimental data was gathered in 1998 and could be outdated or low quality. Unfortunately, open-source data for the pure MDEA is limited, and we can only assume that our optimized ω should result in better binary models.

5.1.3 CO_2

Since the overall objective of this work is the purification of CO_2 from brute biogas production plants, it becomes apparent the need for pure CO_2 parameters

optimization. The experimental data for vapor pressure of CO_2 was also obtained from the Dortmund Data Bank (DDBST) website as shown in Table 1.

The first apparent problem we encountered is the fact that CO_2's critical temperature of 304.21 K could prove to be a challenge when creating the vapor-liquid equilibrium diagrams, since the operating temperatures of the chemical absorption process usually ranges higher than its critical value. In these cases, CO_2 would cease to behave as a standard vapor, displaying characteristics of both liquid and vapor phases, as a supercritical fluid.

Nevertheless, the procedure for this optimization of ω was the same as for pure water and MDEA, since the available experimental data ranges from temperatures lower than its critical value. The optimized ω = 0.2039, which is similar to its literature counterpart of ω = 0.224 and the saturated pressure vs temperature plot can be seen in Figure 7.

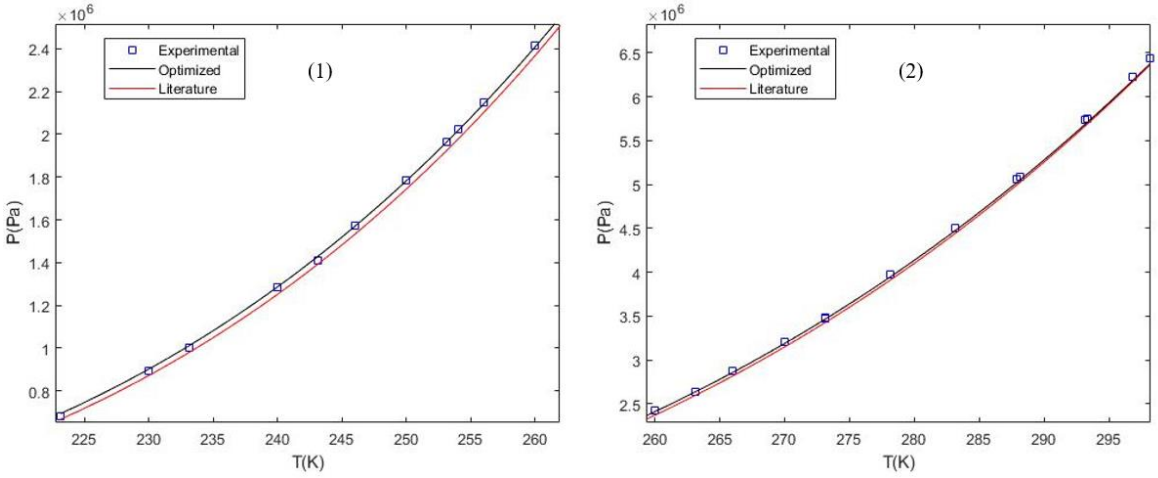

Figure 7. Calculated saturation pressure of CO_2 at lower temperatures (1) and higher temperature (2), while using the optimized acentric factor, w = 0.2039 (-), and its literature counterpart, w = 0.224 (-). The experimental data from DDBST was plotted as well (□).

After analyzing the plots of all three pure components, it is fair to conclude that the classic Peng – Robinson EOS is accurate to calculate the saturated pressure of smaller and simpler molecules such as CO_2 and water, but starts deviating from experimental data whenever the molecules present bigger and more complex chemical

nature, such as MDEA. Still, to evaluate the accuracy of the optimized acentric factor, the error plot and AAD% can be observed in Figure 8.

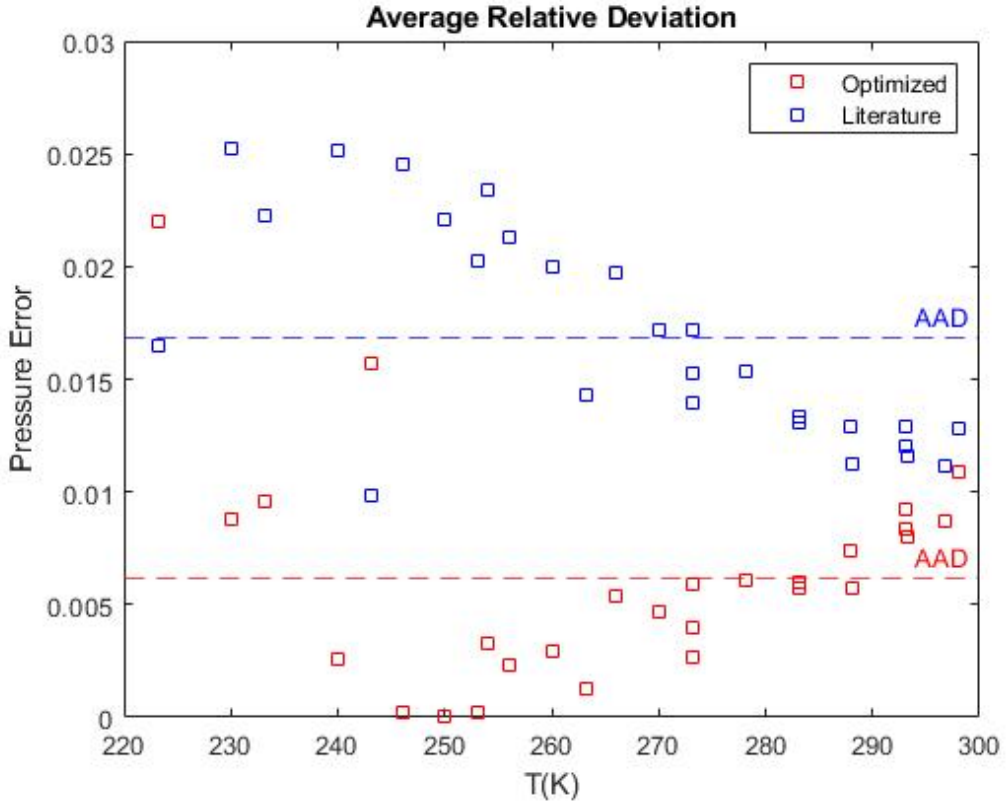

Figure 8. Average absolute deviation of pure CO_2 for the optimized (□) and literature (□) values of ω at different temperatures (K).

The optimized value of ω is shown to calculate more accurate saturated pressure across the entire temperature range, with and AAD% = 0.62, which is very agreeable with the experimental data. In this sense, the literature value of ω also predicted accurate calculated pressure values, with an AAD% = 1.68.

In line of standardizing the procedure for this works thermodynamic algorithm, as well as, overall better AAD% of the optimized ω calculated saturated pressures, the optimized values of all pure components were utilized to calculate all following binary interaction parameters. The overall results obtained for this pure component section can be observed in the following table:

Table 3. Pure components acentric factor optimization and their corresponding AAD%.

Component	Acentric Factor (Optimized)	AAD% (Optimized)	AAD% (Literature)

Water	0.3275	2.81	4.67
MDEA	1.0133	15.86	299.61
CO2	0.2039	0.62	1.68

5.2 MDEA – water using φ – φ approach.

Since the φ – φ approach demonstrated a capable aptitude in predicting the vapor-liquid equilibrium for binary systems of very similar, slightly different and considerably different chemical natures, as previously explained in our "previous models" section, it was the first approach chosen for this thermodynamic algorithm. Since MDEA – water and CO_2 – water systems are more akin to non-ideal systems, the lack of activity coefficient calculations for the components should provide an easier algorithm structure for the model.

The experimental data provides values for system pressure and composition of MDEA in the vapor phase at fixed temperatures of 40 °C, 60 °C, 80 °C and 100 °C from Kim et al. It was separated into two groups: correlation group, which was used inside the objective function minimization algorithms to optimize both interaction parameter, and testing group, which was used to compare the calculated VLE with the experimental data. Therefore, when evaluating the error of our predicted results, two AAD% are obtained, one for the system pressure and another for the composition of MDEA on the vapor phase.

All experimental data of a set temperature was compiled into a single dataset to increase the number of available setpoints for better optimization and error calculations. The setpoints with composition values of zero were removed from the dataset, since their presence creates an error during fugacity mathematical calculations. Finally, since the number of setpoints for the 100 °C was the highest out of the four temperatures, but overall lower than the combined setpoints of 40 °C, 60 °C and 80 °C, the dataset for 100 °C was chosen as the testing group while the other three were selected as the correlation group. Each separate experimental dataset can be found in the appendix section; however, an overview can be seen on the following table:

Table 4. Experimental dataset for MDEA (1) – Water (2).

Temperature (ºC)	Pressure (kPa)	z_1	y_1
40	6.47 – 7.27	7.60E-03 – 1.07E-01	1.00E-06 – 3.00E-05

60	12.87 – 19.77	4.70E-03 – 3.05E-01	3.00E-05 – 4.10E-04
80	31.97 – 47.19	1.00E-08 – 3.06-01	1.00E-08 – 7.40E-04
100	64.18 – 100.40	5.90E-03 – 3.57E-01	3.00E-05 – 1.40E-03

5.2.1 Classic Peng – Robinson Equation of State with non-random mixing rule

With the classic Peng – Robinson with non-random mixing rule there are two parameters that need to be optimized before plotting the vapor – liquid equilibrium at a fixed temperature, the binary interaction parameter, k_{ij}, and the non-random mixture parameter, l_{ij}. As such, the non-random mixture parameter was fixed at zero when optimizing k_{ij} as an initial assumption, since the methodology presented by Poormohammadian et al., only reports a solution procedure to calculate l_{ij}, which leads to believe that k_{ij} was previously known or optimized without the non-random mixing rule. Afterwards, the optimized k_{ij} value is used inside the optimization algorithm for the l_{ij} parameter.

The initial guess for the binary parameter k_{ij} was tested across a range between -0.5 and 0.5, however, positive values higher than 0.02 were incapable of converging to a single value since they resulted in an error caused by a complex root value for the fugacity calculation. Across the values that managed to complete the objective function minimization, the binary parameter for the MDEA – water system converged as k_{ij} = -0.2226 and used for the l_{ij} optimization.

The initial guess for l_{ij} was set as zero, correlating to only random mixing within the components, and was optimized as 0.0273. The relative low value for indicates that this parameter, potentially, is not that influential in the pressure calculations.

Finally, the experimental data at 100 °C was used to plot the VLE diagram, but in lieu of getting a better visualization of the predicted data, the bubble point curve and dew point curve were separated into two different plots, as shown in Figure 9.

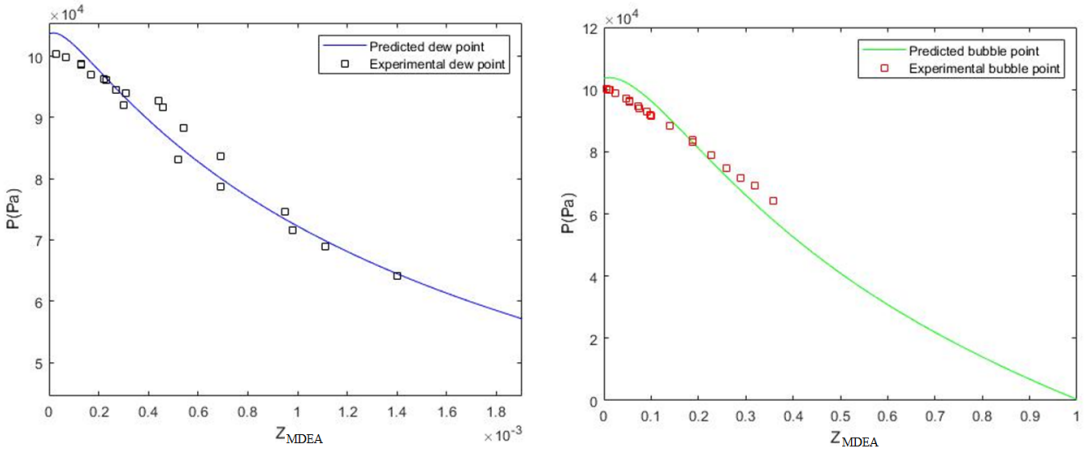

Figure 9. Dew point curve (left) and bubble point curve (right) vapor – liquid equilibrium diagrams of MDEA – water classic Peng – Robinson Equation of State with non-random mixing rule, at 100 °C.

Assuming that the first MDEA composition point of $1x10^{-6}$ as pure water, it can be observed that the predicted saturated pressure of 103619 Pa deviates from the well-established water pressure at 100 °C of 760 mmHg or 101325 Pa, an error of about 2.26%, which is expected since the calculated AAD% for the pure water component was 2.81%. The predicted system pressure and composition errors can be observed on Figure 10.

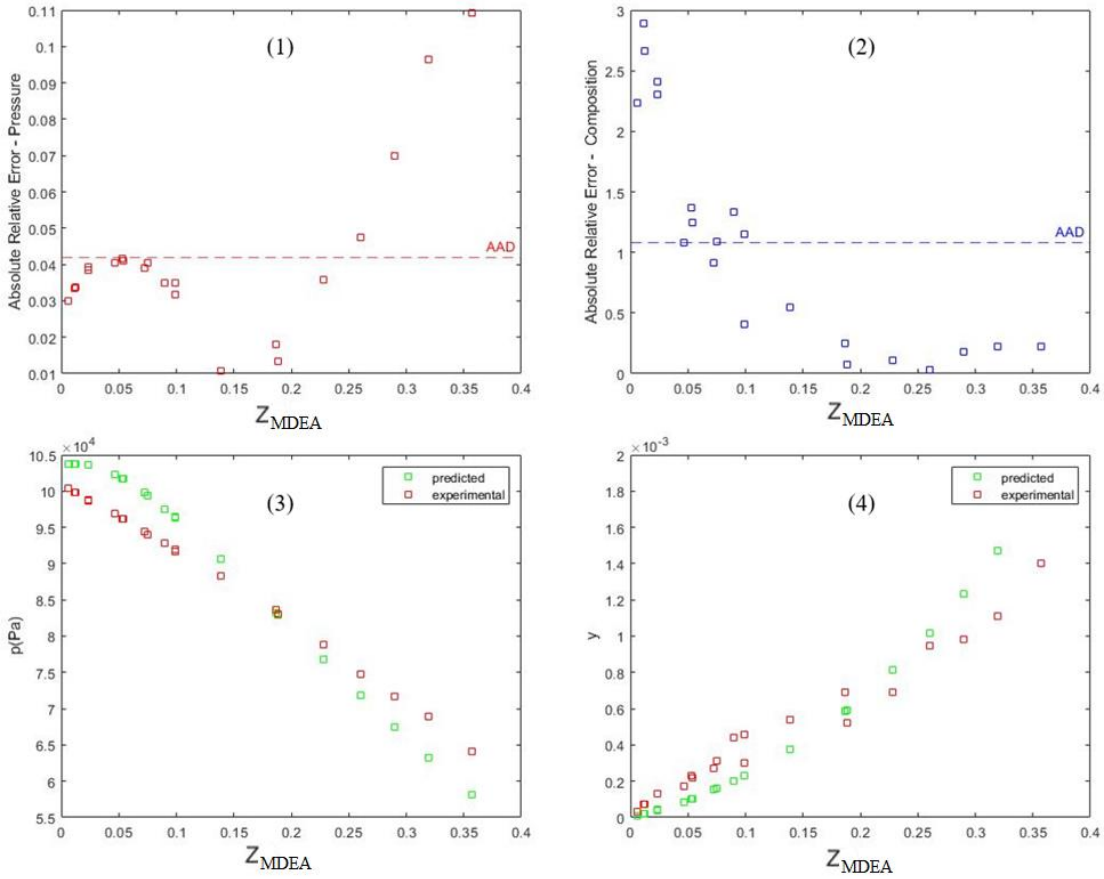

Figure 10. Absolute relative and average deviations for pressure (1), and composition (2), respectively, as well as, comparison of predicted pressure (3) and composition (4) with experimental data at 100 °C, for MDEA – Water classic Peng – Robinson Equation of State with non-random mixing rule.

The pressure plots (1) and (3) illustrates that, overall, predicted system pressure points were fairly agreeable with the experimental data, amassing to an AAD% of 4.61%. However, the absolute error for composition (2) deviates greatly from experimental data, especially on composition containing lower amounts of MDEA, with the highest predicted composition error 2.8 times higher than the supposed experimental data. The AAD% of composition was equal to 100.38%, which could be explained by the fact that these initial setpoints at low amounts of MDEA, with order of magnitude of 10^{-3}, accentuates higher deviations. Another reason is the possibility that our EOS is unable to accurately predict these minute variations of composition, albeit predicting fairly accurate system pressures.

5.2.2 Classic Peng – Robinson EOS with Wong – Sandler mixture rule.

The addition of the Wong – Sandler mixing rule requires the calculation of G^{ex} as was described in Equations 61 and 63. Since Harandi et al., 2021, opted for the e-NRTL activity model, this work computed the excess Gibbs energy at low pressures using the UNIQUAC model, as it was already implemented on the $\gamma - \varphi$ approach.

As explained in section 2.4, the number of first neighbors with respect to a given central atom, Z, was set as equal to eight for all simulations regarding UNIQUAC. The dimension parameters r_i and q_i were calculated using Sandler's functional groups volume and surface area parameters as displayed in the following table (water is considered as functional group because of its unique properties):

Table 5. Group Volume and Surface Area Parameters, R and Q, for use with the UNIQUAC model.

UNIQUAC Parameters	R	Q
CH_3N	1.0746	1.176
CH_2	0.6325	0.7081
$OH_{(p)}$	1.2302	0.8927
Water	1.7334	2.4561

Therefore, according to MDEA structural shape, each molecule consists of four CH_2 groups, two $OH_{(primary)}$ groups and one CH_3N group. The following equation was used to calculate its parameters:

$$r_{MDEA} = \left(4 * r_{CH_2}\right) + \left(2 * r_{OH_{(p)}}\right) + r_{CH_3N}\ ; \quad r_{MDEA} = 6.065 \tag{65}$$

$$q_{MDEA} = \left(4 * q_{CH_2}\right) + \left(2 * q_{OH_{(p)}}\right) + q_{CH_3N}\ ;\ q_{MDEA} = 5.7938 \tag{66}$$

In that regard, the UNIQUAC equation contains only two adjustable parameters τ_{12} and τ_{21}, each dependent on two adjustable parameters, u_{12}^0, u_{12}^T, u_{21}^0 and u_{21}^T, for a total of four adjustable parameters. With the additional binary interaction parameter, k_{ij}, from the classic Peng – Robinson EOS, each binary system will have five adjustable parameters. As such, this work developed two strategies of optimization:

1) Sequential optimization: Setting $k_{ij} = 0$, $u_{12}^0 = 100$, $u_{12}^T = 0$, $u_{21}^0 = 100$, $u_{21}^T = 0$ and optimizing the four UNIQUAC parameters, u_{12}^0, u_{12}^T, u_{21}^0 and u_{21}^T. Afterwards, using these optimized parameters for k_{ij} optimization.
2) Simultaneous optimization: With the same initial values, optimizing all five parameters simultaneously.

5.2.2.1 Sequential Strategy – Results

This strategy aims to focus on the mixing rule as the center of optimization, since the excess Gibbs energy calculation is a precursor to the EOS parameters definition (Equation 61). UNIQUAC parameters were compared to experimental data assuming the effect of the binary interaction parameter (Equation 63) is negligible.

The group separation of the experimental data into correlation and testing follows the same methodology applied to the classic Peng – Robinson EOS with non-random mixing rule, as to allow for comparisons between both models. Once again, the experimental data at 100 °C was used to plot the VLE diagram and the bubble point curve and dew point curve were separated into two different plots, as shown in Figure 11.

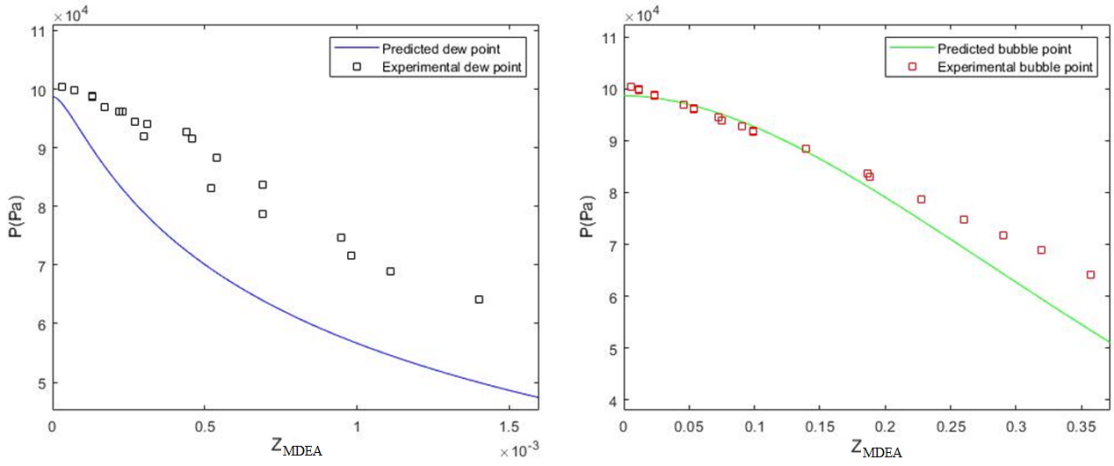

Figure 11. Dew point curve (left) and bubble point curve (right) vapor – liquid equilibrium diagrams of MDEA – water classic Peng – Robinson Equation of State with Wong – Sandler mixing rule, at 100 °C (Sequential Strategy).

The optimized UNIQUAC parameters resulted in $u_{12}^0 = -404.0766$, $u_{12}^T = 11.084$, $u_{21}^0 = 455.8335$, $u_{21}^T = -10.8765$ and binary interaction parameter, $k_{ij} = 0.0418$. The predicted water saturated pressure of the Wong – Sandler model with the

first strategy was 98749.4 Pa, an error of about 2.54%, which is higher than the one from non-random mixing rule.

The predicted bubble point curve can be observed as agreeing with the experimental data, but the same cannot be said for the predicted dew point curve, where a clear deviation is apparent. This deviation could be associated with the predicted saturated pressure being lower than the established water pressure at 100 °C of 101325 Pa, since the curve also tends towards predicting lower pressures than the experimental data. The predicted system pressure and composition errors can be observed on Figure 12.

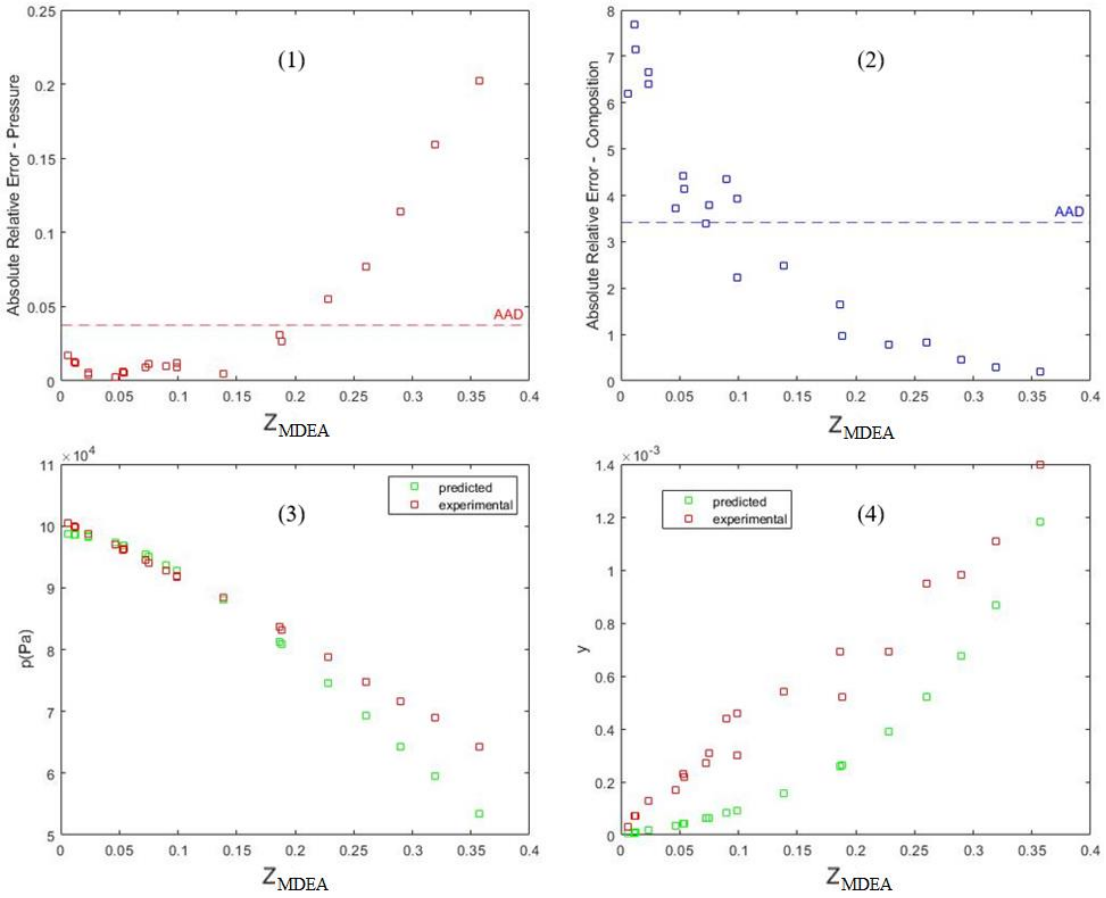

Figure 12. Absolute relative and average deviations for pressure (1), and composition (2), respectively, as well as, comparison of predicted pressure (3) and composition (4) with experimental data at 100 °C, for MDEA – Water classic Peng – Robinson Equation of State with Wong - Sandler mixing rule (Sequential Strategy).

As can be observed in plots (1) and (3), the predicted pressure for the MDEA-water system agrees with the experimental data, amassing an AAD% of 3.76%, which is lower than the non-random mixing rule of 4.61%. However, the composition AAD%

was equal to 341.26%, which is more than three times higher than 100.38% from the non-random mixing rule, with a maximum deviation of 7.68 times higher than experimental data. It is safe to conclude that the increase in pressure accuracy directly results in a decrease in composition accuracy for the thermodynamic model.

5.2.2.2 Simultaneous Strategy – Results

This strategy aims to correlate all interaction effects present in the experimental data as a basis for parameter optimization. Therefore, all experimental data group separation follows the same principles previously described, but the optimization includes all UNIQUAC parameters and the EOS binary interaction parameter. The VLE diagram at 100 °C can be observed in Figure 13.

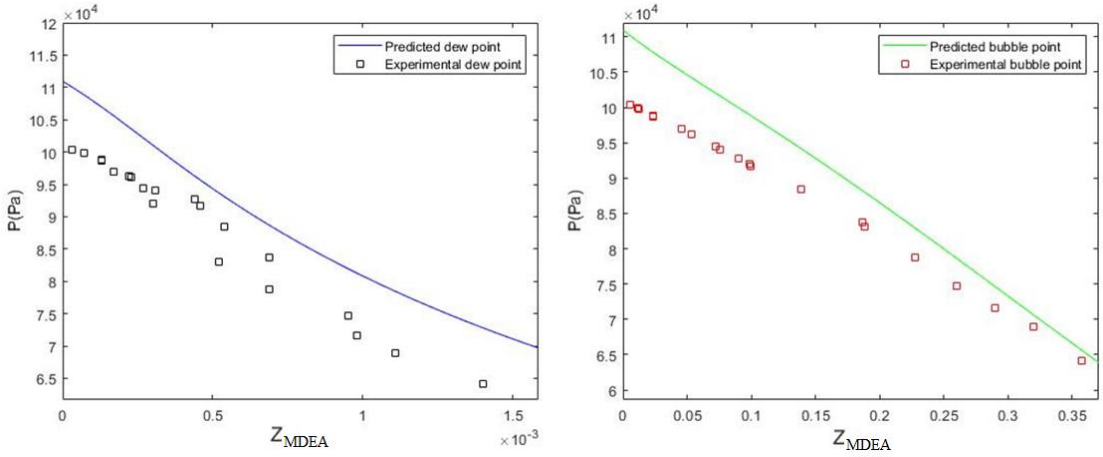

Figure 13. Second Strategy - Dew point curve (left) and bubble point curve (right) vapor – liquid equilibrium diagrams of MDEA – water classic Peng – Robinson Equation of State with Wong - Sandler mixing rule, at 100 °C.

The optimized UNIQUAC parameters resulted in $u_{12}^{0} = -234.2841$, $u_{12}^{T} = 1.0499$, $u_{21}^{0} = 266.4326$, $u_{21}^{T} = 0.1966$ and binary interaction parameter, $k_{ij} = -0.0715$. The predicted water saturated pressure of the Wong – Sandler model with the second strategy was 110940 Pa, an error of about 9.49%, which is higher than both first strategy and non-random mixing rule models. The predicted system pressure and composition errors can be observed on Figure 14.

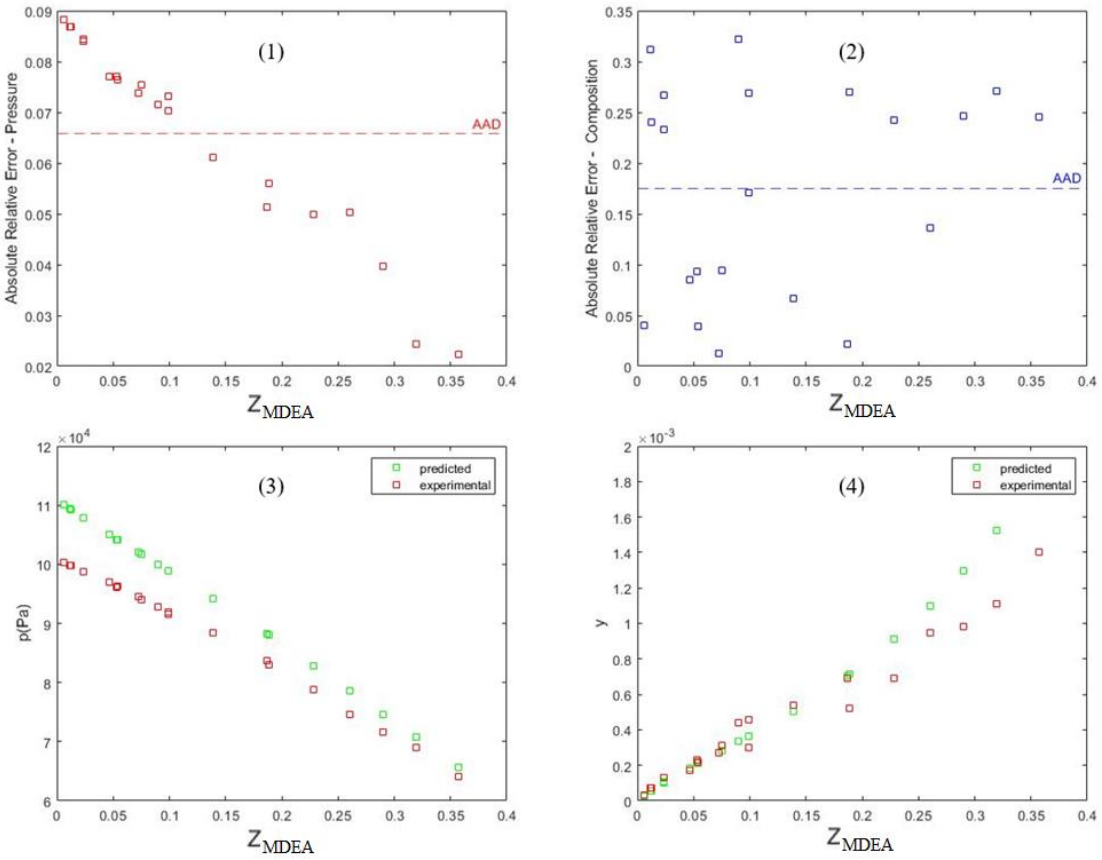

Figure 14. Absolute relative and average deviations for pressure (1), and composition (2), respectively, as well as, comparison of predicted pressure (3) and composition (4) with experimental data at 100 °C, for MDEA – Water classic Peng – Robinson Equation of State with Wong – Sandler mixing rule (Second Strategy).

It becomes apparent that predicted composition accuracy increased drastically, while predicted pressure accuracy decreased when compared to both the first strategy of Wong – Sandler mixing rule and non-random mixing rule. The AAD% for predicted pressure and composition were 6.57% and 17.51%, respectively, which corroborate this "see-saw" effect, where increasing precision in pressure decreases composition accuracy and vice versa. The choice in optimization strategy was shown to greatly influence parameter values, as well as, overall thermodynamic model accuracy.

5.3 MDEA – water using γ – φ approach

The methodology for experimental data group separation follows the same procedure as the one described in the $\varphi - \varphi$ approach. The initial value for binary interaction and UNIQUAC parameters were set as $k_{ij} = 0, u_{12}^0 = 100, u_{12}^T = 0, u_{21}^0 =$

100, $u_{21}^{T} = 0$. The parameter optimization will follow both strategies as described in section 3.2.2.

5.3.1 Classic Peng – Robinson Equation of State with non – random mixing rule

The equations of state selected for the $\gamma - \varphi$ approach is the same as $\varphi - \varphi$ approach to allow structure similarity for result comparison. Since the $\gamma - \varphi$ approach always require calculations of excess Gibbs free energy via UNIQUAC model, the optimization strategies were also applied to this model with the addition of the non-random binary interaction parameter, l_{ij}. Therefore, the sequential strategy optimizes the parameters in the following order: first the UNIQUAC parameters, followed by both interaction parameters, k_{ij} and l_{ij}.

The sequential strategy to optimize UNIQUAC parameters before the binary interaction parameters resulted in a $k_{ij} = -5.7881$ and $l_{ij} = -33.9484$, which deviates from its expected value range. The UNIQUAC parameters were optimized as $u_{12}^{0} = 506.4185, \quad u_{12}^{T} = 0.0011, \quad u_{21}^{0} = -319.581, \quad u_{21}^{T} = -0.0037$ with a corresponding pressure and composition AAD% of 2.25% and 21.81%. Even though these results show potential, this is an example of incorrect parameters since it gives accurate predictions towards the selected experimental data but the binary interaction parameters anomaly would give inaccurate results towards new data. Therefore, this work shall refrain from displaying the resulting plots of this strategy.

The simultaneous optimization strategy did not show a similar anomaly, allowing its results to be considered as valid. The bubble point and dew point curves can be seen below.

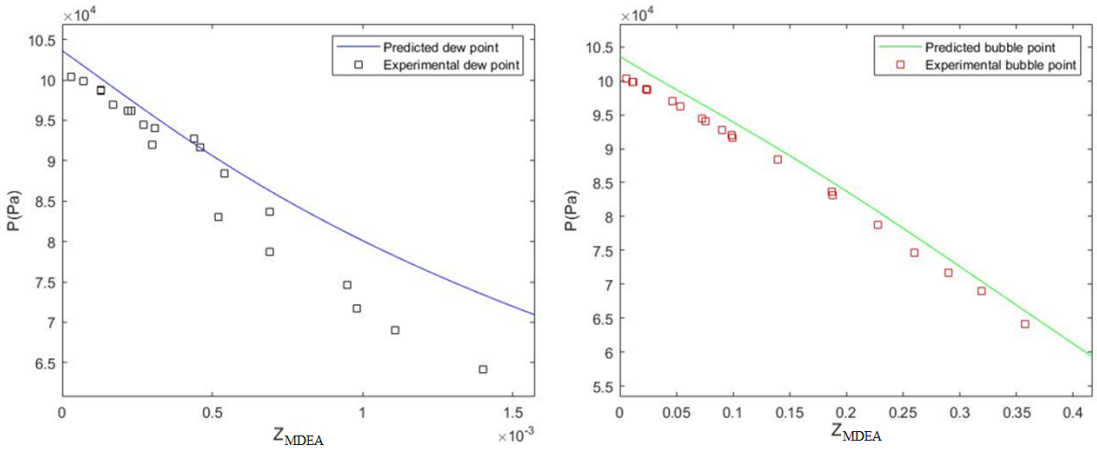

Figure 15. Dew point curve (left) and bubble point curve (right) for γ – φ approach vapor – liquid equilibrium diagrams for γ – φ approach MDEA – water classic Peng – Robinson Equation of State and non-random mixing rule, at 100 °C (Simultaneous Strategy).

The binary interaction and UNIQUAC parameters were optimized as $k_{ij} = -0.0045$, $l_{ij} = -0.0047$, $u_{12}^{0} = 507.5088$, $u_{12}^{T} = 0.0042$, $u_{21}^{0} = -320.239$, $u_{21}^{T} = 0.0001$. The predicted water saturated pressure was 103600 Pa, an error of 2.25%, which is almost the same as predicted by the $\varphi - \varphi$ approach with classic Peng – Robinson EOS and non-random mixing rule. The predicted system pressure and composition errors can be observed on Figure 16.

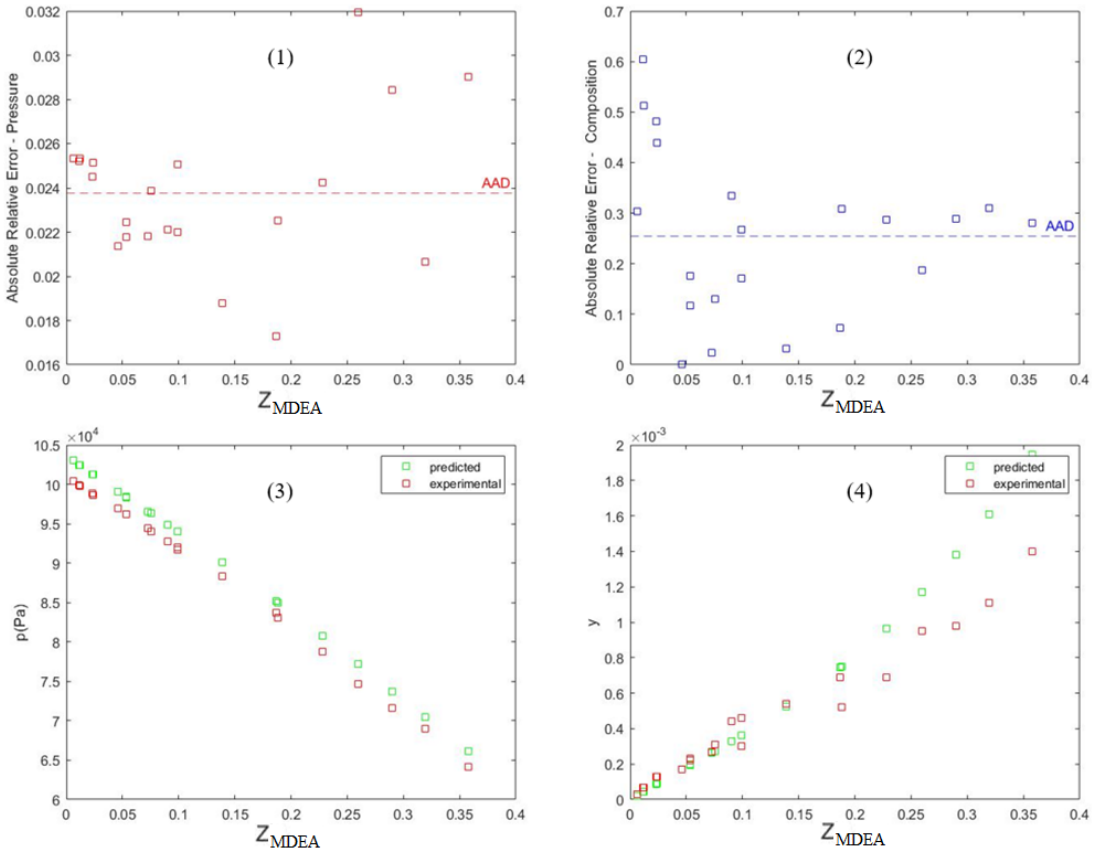

Figure 16. Absolute relative and average deviations for pressure (1), and composition (2), respectively, as well as, comparison of predicted pressure (3) and composition (4) with experimental data at 100 °C, for $\gamma - \varphi$ approach MDEA – Water classic Peng – Robinson Equation and non-random mixing rule (Simultaneous Strategy).

The predicted AAD% for both pressure and composition were equal to 2.38% and 25.37%, respectively, both higher than its sequential strategy counterpart but without the binary interaction parameters anomaly. This fact shows the importance of knowing the expected behavior of optimized parameters, in any thermodynamic model, to avoid false values. The simultaneous strategy gave the lowest reported absolute average deviation for predicted pressure, but the composition error is still higher than what was obtained by the $\varphi - \varphi$ approach classic Peng – Robinson with Wong – Sandler mixing rule (simultaneous strategy).

5.3.2 Classic Peng – Robinson EOS with Wong – Sandler mixture rule.

Opposite to the non-random mixing rule, the simultaneous strategy of optimization resulted in a $k_{ij} = -13.257$, which greatly deviates from its expected

value range. The UNIQUAC parameters were optimized as $u_{12}^{0} = -114.1834$, $u_{12}^{T} = -5.0021$, $u_{21}^{0} = -82.5110$, $u_{21}^{T} = 13.6729$, but should be discarded as a result of being incorrect.

On the other hand, the sequential strategy resulted in an optimized $k_{ij} = -0.6285$, which allows the results to be taken into consideration. As such, the VLE diagrams can be observed as follows.

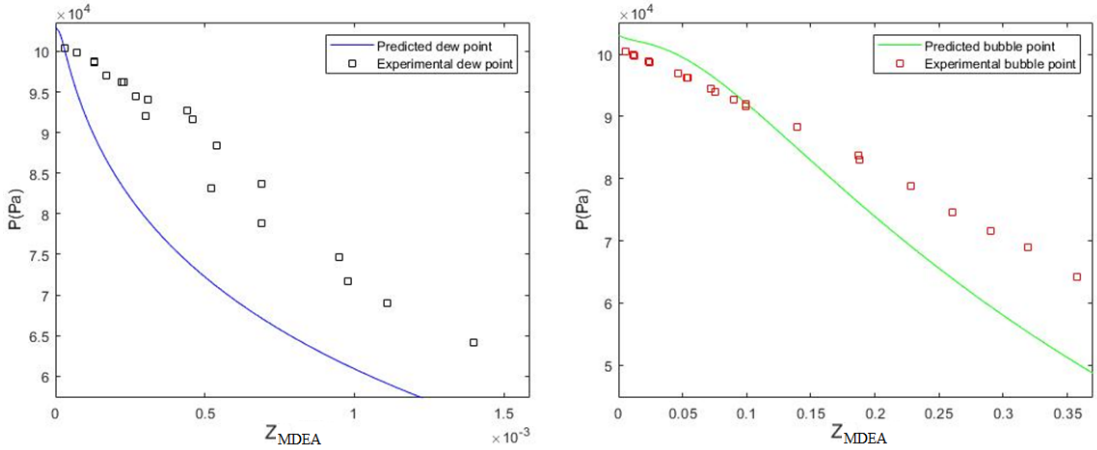

Figure 17. Dew point curve (left) and bubble point curve (right) for γ – φ approach vapor – liquid equilibrium diagrams of MDEA – water classic Peng – Robinson Equation of State with Wong – Sandler mixing rule, at 100 °C.

The UNIQUAC parameters were optimized as $u_{12}^{0} = -41.4703$, $u_{12}^{T} = -5.6713$, $u_{21}^{0} = -181.273$, $u_{21}^{T} = 13.9313$. The predicted water saturated pressure was 102990 Pa, an error of 1.64%, the lowest error throughout all models. The predicted system pressure and composition errors can be observed on Figure 18.

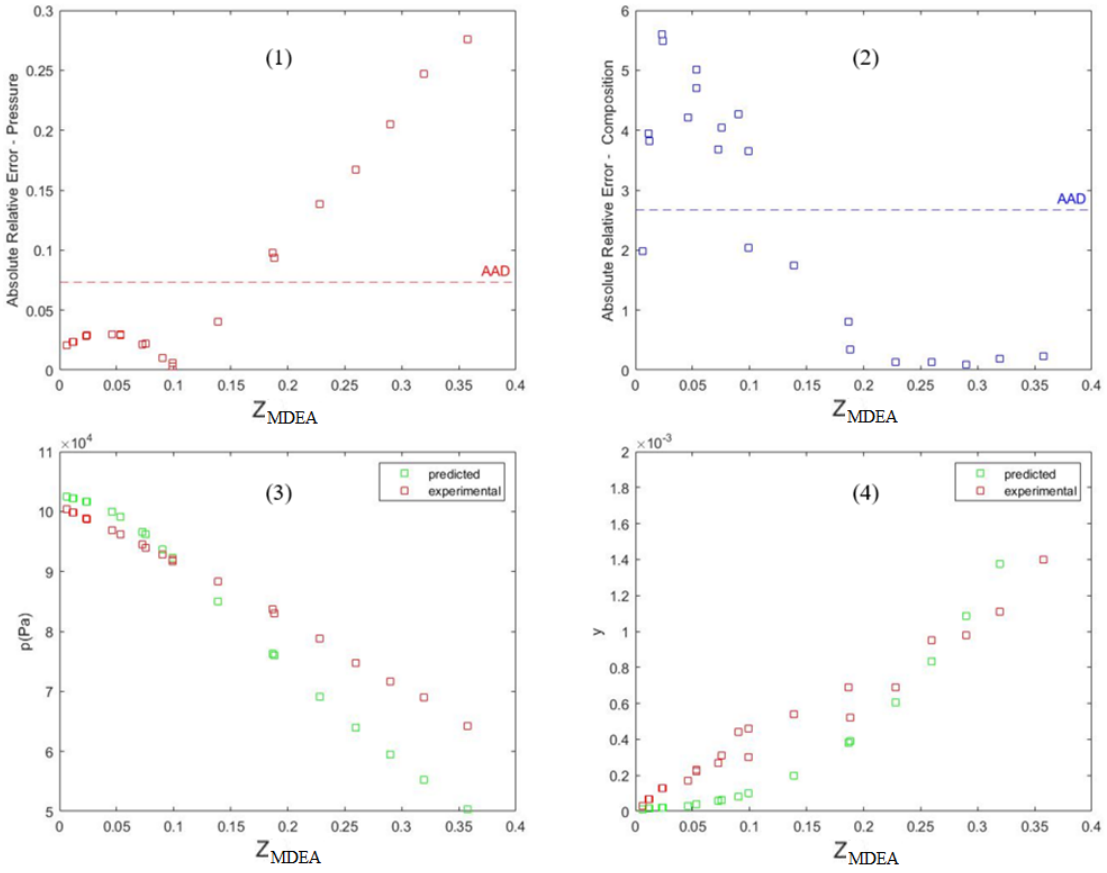

Figure 18. Absolute relative and average deviations for pressure (1), and composition (2), respectively, as well as, comparison of predicted pressure (3) and composition (4) with experimental data at 100 °C, for γ – φ approach MDEA – Water classic Peng – Robinson Equation and Wong – Sandler mixing rule (Sequential Strategy).

The AAD% for both pressure and composition were equal to 7.34% and 267.27%, respectively, the highest-pressure error and a very high composition error, indicating that the $\gamma - \varphi$ approach Peng – Robinson and Wong – Sandler mixture isn't an ideal model for this application. This could be related to the fact that the UNIQUAC parameters are being used for both excess Gibbs energy used on the Wong – Sandler mixing rule and for the activity coefficient of the liquid phase, correlating the dimensional parameters with two regions of optimization, causing it to give inadequate results.

The overall results of all applied models to the binary system MDEA – water can be observed on the following table:

Table 6. MDEA – water optimized parameters and associated absolute average deviation for all presented models.

Models (Temperature = 100 °C)	k_{ij}	l_{ij}	u_{12}^{0}	u_{21}^{0}	u_{12}^{T}	u_{21}^{T}	AADP% (Pressure)	AADC% (Composition)
$\varphi - \varphi$ PRNR	-0.2226	0.0273	–	–	–	–	4.61	100.38
$\varphi - \varphi$ PRWS (sequential)	0.0418	–	-404.077	455.8335	11.084	-10.8765	3.76	341.26
$\varphi - \varphi$ PRWS (simultaneous)	-0.0715	–	-234.284	266.4326	1.0499	0.1966	6.57	17.51
$\gamma - \varphi$ PRNR* (sequential)	-5.7881	-33.9484	506.4185	-319.581	0.0011	-0.0037	2.25	21.81
$\gamma - \varphi$ PRNR (simultaneous)	-0.0045	-0.0047	507.5088	-320.239	0.0042	0.0001	2.38	25.37
$\gamma - \varphi$ PRWS (sequential)	-0.6285	–	-41.4703	-181.273	-5.6713	13.9313	7.34	267.27
$\gamma - \varphi$ PRWS* (simultaneous)	-13.257	–	-114.183	-82.511	-5.0021	13.6729	–	–
PRNR = Classic Peng – Robinson with non-random mixing rule; PRWS = Classic Peng – Robinson with Wong – Sandler mixing rule								
Sequential = Optimization of UNIQUAC parameters first, followed by the optimization of binary interaction parameters								
Simultaneous = Optimization of both UNIQUAC and binary interaction parameters at the same time								
* = Overfitted parameters								

It becomes apparent that any chosen approach and equation of state, as well as, the strategy at which the operator decides to do the optimization, greatly influences interaction parameter values and the overall accuracy of the thermodynamic model. The possibility of erroneous values establishes a need to fundamentally understand the physical significance of optimized parameters as demonstrated by the $\gamma - \varphi$ PRNR (sequential strategy) model.

Both $\varphi - \varphi$ and $\gamma - \varphi$ approaches proved to be effective at modeling the binary MDEA – water system, with $\varphi - \varphi$ PRWS (simultaneous strategy) and $\gamma - \varphi$ PRNR (simultaneous strategy), the former being more accurate to predict system pressure and the latter more accurate to predict system composition. Predicted saturated pressure of components was shown to agree with the associated AAD% obtained on the pure components optimization, demonstrating that classic Peng – Robinson's lack of accuracy could propagate this error for more complex systems.

6. Conclusion

The optimization of interaction parameters pertaining the MDEA – Water binary system were evaluated by a bubble pressure algorithm thermodynamic model using both φ – φ and γ – φ approaches, classic Peng–Robinson with the non-random mixing rule and Wong-Sandler mixing rule EOS. The calculated acentric factor, ω, of water, CO_2 and MDEA were 0.3275, 0.2039 and 1.0133 respectively with lower vapor pressure AAD than literature values. The $\gamma - \varphi$ approach was sensitive in regards to the optimization strategy of parameters, displaying cases of thermodynamically false values for both PRNR and PRWS equations of state. The PRNR with simultaneous strategy gave accurate predictions regarding vapor pressure, with AAD% = 2.38%, on the other hand, the composition errors were considerable at AAD% = 25.37%. The $\phi - \phi$ approach did not suffer from incorrect parameter estimation across models, displaying the best overall result via classic Peng – Robinson with Wong – Sandler mixing rule and simultaneous parameter optimization strategy. The parameters were optimized as $u_{12}^0 = -234.2841$, $u_{12}^T = 1.0499$, $u_{21}^0 = 266.4326$, $u_{21}^T = 0.1966$, $k_{ij} = -0.0715$, with vapor pressure AAD% = 6.57% and composition AAD% = 17.51%. The choice in optimization strategy was shown to greatly influence parameter values and model accuracy, probably as a result of our minimizing function's inability to find a global minimum, instead of a local minimum. For future works, the substitution of the classic PR-EOS, for its more robust and complex α parameters calculation counterparts, may reduce the predicted errors associated with pressure, from pure component saturated pressure to higher complexity systems. More complex minimization functions to find global minimum, such as, particle swarm optimization, could prevent local minimum predictions. The acentric factor optimization could be tested to include the coefficients of its quadratic equation as parameters, to examine their effects on pressure errors.

7. Bibliography References

1. ABDEEN, F. R. H., MEL, M., JAMI, M. S., IHSAN, S. I., ISMAIL, A. F. A review of chemical absorption of carbon dioxide for biogas upgrading, Chinese Journal of Chemical Engineering, 24 (2016) 693-702.
2. COQUELET, C., CHAPOY, A., RICHON, D. Development of a New Alpha Function for the Peng –Robinson Equation of State: Comparative Study of Alpha Function Models for Pure Gases (Natural Gas Components) and Water-Gas Systems, vol. 25, no. 1, 2004.
3. GAMBA, S., PELLEGRINI, L.A. Biogas upgrading: Analysis and comparison between water and chemical scrubbings, Chem. Eng. 32 (2013) 1273–1278.
4. GAMBA, S., PELLEGRINI, L.A., LANGÈ, S. Energy analysis of different municipal sewage sludge-derived biogas upgrading techniques, Chem. Eng. 37 (2014) 829–834.
5. GAUR, A., PARK, J.-W., MAKEN, S., SONG, H.-J., PARK, J.-J. Landfill gas (LFG) processing via adsorption and alkanolamine absorption, Fuel Process. Technol. 91 (2010) 635–640.
6. GÜNTHER, L. Method and device for separating methane and carbon dioxide from biogas, US8231706 B2, 2012.
7. JUNIOR, A. D. N. F., ETCHEBEHERE, C., PERECIN, D., TEIXEIRA, S., WOODS, J. Advancing anaerobic digestion of sugarcane vinasse: Current development, struggles and future trends on production and end-uses of biogas in Brazil, Renewable and Sustainable Energy Reviews 157 (2022) 112045.
8. KIM, I., SVENDSEN, F.H., BORRESEN, E. Ebulliometric Determination of Vapor-Liquid Equilibria for Pure Water, Monoethanolamine, N-Methyldiethanolamine, 3-(Methylamino)-propylamine, and Their Binary and Ternary Solutions, J. Chem. Eng. Data 2008, 53, 2521-2531.
9. KONTOGEORGIS, G. M., GANI, R. Computer Aided Property Estimation for Process and Product Design, 19. Elsevier B.V., pp. 75–83, 2004.

10. MATHIAS, P.M., COPEMAN, T.W. Extension of the Peng-Robinson equation of state to complex mixtures: Evaluation of the various forms of the local composition concept, Fluid Phase Equilib 13 (C) (1983) 91–108.
11. MOREIRA, L. C., BORGES, P. O., CAVALCANTE, R. M., YOUNG, A. F. Simulation and economic evaluation of process alternatives for biogas production and purification from sugarcane vinasse, Renewable and Sustainable Energy Reviews 163 (2022) 112532.
12. NOLL, O., VALTZ, A., RICHON, D., GETACHEW-SAWAYA, T., MOKBEL, I., JOSE, J. Vapor pressure and liquid densities of N-methylethanolamine, diethanolamine, and N-methyldiethanolamine, ELDATA: Int. Electron. J. Phys-Chem. Data. 1998, 4, 105-120.
13. OKAMURA, L. A., SAKUMA, A. C., COSTA, B. J., PILISSÃO, C., FONTANA, J. D., COSTA NETO, P. R. Landfill biogas purification, Int. J. Oil, Gas and Coal Technology, Vol. 17, No. 4, 2018.
14. OLIVEIRA, L. G., CREMONEZ, P. A., MACHADO, B., DA SILVA, E. S., SILVA, F. E. B., CORRÊA, G. C. G., LOPEZ, T. F. M., ALVES, H. J. Updates on biogas enrichment and purification methods: A review, Can. J. Chem. Eng. 2022, 1.
15. PARSAEE, M., KIANI, M. K. D., KARIMI, K. A review of biogas production from sugarcane vinasse, Biomass and Bioenergy 122 (2019) 117–125.
16. PENG, D. Y., ROBINSON, D. B. A New Two-Constant Equation of State, Ind. Eng. Chem., Fundam., Vol. 15, No. 1, 1976.
17. PERALTA, N.G. Mass transfer in chemical engineering processes - Chapter 7 – Removal of H2S and CO2 from biogas by amine absorption, Ingeniería e Investigación 33 (2013) 75–76.
18. POORMOHAMMADIAN, S. J., LASHANIZADEGAN, A., SALOOKI, M. K. Modelling VLE data of CO2 and H2S in aqueous solutions of N-methyldiethanolamine based on non-random mixing rules, International Journal of Greenhouse Gas Control, 2015, 45, 87-97.

19. PRAUSNITZ, J. M., ABRAMS, D. S. Statistical Thermodynamics of Liquid Mixtures: A New Expression for the Excess Gibbs Energy of Partly or Completely Miscible Systems, AlChE Journal, Vol. 21, No. 1, 1975.
20. RIO DE JANEIRO, National Oil, Natural Gas and Biofuels Agency, ANP Resolution Nº 685 June, 29 of 2017. Establishes the rules for approval of quality control and the specification of biomethane from landfills and sewage treatment plants intended for vehicular use and residential, industrial and commercial installations to be sold throughout the national territory. ANP, Rio de Janeiro, Brazil 2017.
21. SANDLER, S. I. Chemical, Biochemical, and Engineering Thermodynamics, 5th edition, ISBN: 978-0-470-50479-6, 2017.
22. THOMSEN, K., RASMUSSEN, P. Modeling of vapor – liquid – solid equilibrium in gas – aqueous electrolyte systems, Chemical Engineering Science 54 (1999) 1787 – 1802.
23. TREBBLE, M.A., BISHNOI P.R., ENGINEERING, P. Development of a New Four-Parameter Cubic Equation of State, Fluid Phase Equilib. 35 (1987) 1–18.
24. TWU, C.H., COON, J.E., CUNNINGHAM J.R. A new generalized alpha function for a cubic equation of state Part 1. Peng-Robinson equation, Fluid Phase Equilib. 105 (1) (1995) 49–59.
25. WONG, D. S. H., SANDLER, S. I. A Theoretically Correct Mixing Rule for Cubic Equations of State, AlChE Journal, Vol. 38, No. 5, 1992.
26. ZIABAKHSH-GANJI, Z., KOOI, H. An equation of state for thermodynamic equilibrium of gas mixtures and brines to allow simulation of the effects of impurities in subsurface CO2 storage, Int. J. Greenhouse Gas Control 11S, S21–S34, 2012.

8. Appendix

Table 7. Vapor pressure of water experimental data from DDBST.

Temperature (K)	Pressure (kPa)
293.15	2.40E+00
303.15	4.27E+00
313.15	7.33E+00
323.15	1.23E+01
333.15	1.99E+01
343.15	3.12E+01
412.75	3.57E+02
432.85	6.13E+02
451.25	9.60E+02
463.15	1.26E+03
473.35	1.56E+03
482.55	1.89E+03
492.65	2.30E+03
504.15	2.85E+03
507.77	3.04E+03
521.28	3.85E+03
535.18	4.85E+03
541.49	5.36E+03
552.6	6.37E+03
557.97	6.90E+03
561.69	7.29E+03
571.31	8.37E+03

Table 8. Vapor pressure of MDEA experimental data from Noll et al.

Temperature (K)	Pressure (kPa)
293.69	6.10E-04
303.56	1.48E-03
303.56	1.47E-03
313.46	3.42E-03

313.47	3.47E-03
323.3	7.98E-03
323.3	7.95E-03
333.23	1.81E-02
333.23	1.81E-02
343.04	3.93E-02
343.06	3.97E-02
351.94	7.71E-02
351.97	7.68E-02
352.96	8.15E-02
353	8.09E-02
361.94	1.57E-01
361.97	1.57E-01
371.87	2.90E-01
371.89	2.91E-01
381.89	5.45E-01
381.9	5.28E-01
381.91	5.21E-01
391.96	8.84E-01
391.97	8.81E-01
401.96	1.48E+00
401.97	1.48E+00

Table 9. Vapor pressure of CO_2 experimental data from DDBST.

Temperature (K)	Pressure (kPa)
223.15	6.79E+02
230	8.95E+02
233.15	1.00E+03
240	1.28E+03
243.15	1.41E+03
246	1.57E+03
250	1.78E+03
253.15	1.97E+03
254	2.02E+03
256	2.15E+03
260	2.42E+03
263.15	2.63E+03
266	2.87E+03

270	3.20E+03
273.15	3.48E+03
273.15	3.48E+03
273.15	3.49E+03
278.15	3.97E+03
283.15	4.50E+03
283.15	4.50E+03
287.91	5.06E+03
288.15	5.08E+03
293.15	5.73E+03
293.15	5.74E+03
293.34	5.75E+03
296.79	6.23E+03
298.15	6.44E+03